# A STANDARDIZED REMOTE SENSING METHODOLOGY FOR MAPPING MINERALOGICAL MINING WASTE ANOMALIES ACROSS EUROPEAN COUNTRIES USING PRINCIPAL COMPONENT ANALYSIS AND GIS DATA INTEGRATION

**Anca-Marina VÎJDEA[1,2], Stefan SOMMER[2]**

*[1]Geological Institute of Romania; 1 Caransebes St., 012271 Bucharest, Romania*
*e-mail: anca.vijdea@igr.ro*
*[2]Joint Research Centre of the European Commission, Institute for Environment and Sustainability; 1 Via Enrico Fermi, 21020 Ispra (Va), Italy*

DOI: 10.xxxx

**Abstract.** This paper presents a methodology based on medium resolution satellite images (Landsat Thematic Mapper and Enhanced Thematic Mapper), adapted and further developed from a variant of a Principal Components Analysis used for geological exploration, which took into consideration the spectral bands in the visible and infrared wavelengths where the minerals of interest exhibited diagnostic features. The method was developed to be applied for an inventory of mining wastes at pan-European scale and was successfully tested in known mining regions with closed exploitations in Upper Silesia (Poland), Romania and Slovakia. The results were validated against European (CORINE Land Cover) and national data sets. A Mining Anomaly Index was computed at catchment scale, to determine the most vulnerable river basins from which pollutants from the extractive industry could be further transported to the seas. In view of the present increased demand for metals and critical raw materials, the principles of the described methodology could be applied to the new satellite sensors, with increased ground and spectral resolution.

**Key words:** mining waste; Landsat; Feature-Oriented Principal Component Selection (FPCS); Mining Anomaly Index; Poland; Romania; Slovakia

## 1. INTRODUCTION

In the last ten years of the XX$^{th}$ century many mines were closed in Europe, starting in Western and Central European countries, and followed by Eastern European countries which joined the EU. Europe's intention was to protect its environment, the rivers and the seas from undesired pollution caused by sometimes uncareful exploitation and/or by natural transformation of minerals exposed to weathering by mining works. It was believed that the natural demand for metals and other natural mineral resources could be satisfied in the future by imports from very rich deposits located on other continents (Constantinescu and Atanasiu, 2017).

The necessity to inform the general public and governments about the potential risks related to active and closed mines was reinforced after the mining accidents of Aznacóllar (Spain – 1989), Baia Bare and Baia Borşa (Romania – 2000). The concern about the cross-border effects of such events led to the approval of a new Directive of the European Parliament and of the Council on the management of waste from extractive industries in 2006 (2006/21/EC). This requires that the Member States make inventories of closed mining facilities that might cause threat to the environment and human health within a defined time period.

A great deal of information exists in countries of the European Union regarding active and closed mining facilities.

This information is often not homogeneous and lacks standardization in terms of parameterization, formats and geographical reference systems and can be outdated and scattered between different users and owners (Sommer, 2004). The completion by detailed geochemical investigation and the integration and the harmonization of data at country level in order to assess the areas at risk is a time-consuming task, implying increased costs for the responsible ministries and national organizations/agencies in charge of this. Harmonizing the information at European level could be a very difficult task because of gaps and inconsistencies.

In this paper we propose a way of making up risk inventories at national level by providing a uniform, standardized base layer at European level of areas which present high concentration in iron oxides and secondary alteration minerals characterized by the hydroxyl-metal bond. These areas correspond to accumulation of mining wastes, landfills from various industries and sites with high concentration of gaseous/particle emissions. Identifying these areas on satellite images of medium spectral and spatial resolution (Landsat Thematic Mapper TM/Enhanced Thematic Mapper ETM) represents the most cost-effective solution for a rapid screening of zones characterized by an intense mining and/or industrial polluting activity at regional or country level. It allows the identification of areas where the mining dumps from closed facilities have already been remedied and vegetation has begun to grow again, emphasizing that the existing data are outdated. This method allows the detection of industrial sites that are emitting high levels of gaseous/particle emissions in the surrounding environment. This way a prioritization of the areas where detailed geochemical and other type of investigations are necessary in order to perform a risk assessment analysis can be obtained. The costs at national scale are reduced by concentrating the sample collection and ground/laboratory assays only to these highly "anomalous areas" that are previously identified on satellite images.

The uniform and standardized, georeferenced layer of remote sensing based anomalies showing the areas enriched in iron oxides (FeOx) and hydroxyl-bearing (OH) secondary alteration minerals, indicating accumulations of mining-originated waste material, could serve as the basis for checking, updating and filling information gaps in national mining inventories across the European continent. The FeOx and OH anomalies are obtained by processing Landsat TM images with a method based on Principal Components Analysis (PCA), a method applied for mineral exploration with success (Crosta and McMoore, 1989, Louglin, 1990, 1991). These anomalies are even better suited for mapping mining wastes due to the larger quantity of exposed material than in the case of rock outcrops and subtle hydrothermal alteration features for which it is currently applied. Basically, the iron oxides are mapped based on the difference in reflectance in the Thematic Mapper pair bands TM1-TM3, while hydroxyl-bearing minerals are mapped by exploiting differences in TM5-TM7.

In this study we describe the method originally developed for exploration geology and adapted to be applied at a pan-European scale on full satellite frames in an operational way. Three big areas in Central and Eastern Europe within Poland, Slovakia and Romania were used for testing and applying the method.

## 2. STUDY AREA AND DATA SETS

### 2.1. Geographical setting

The study area is covered by a series of 8 multi-temporal Landsat TM/ETM scenes, making up a total of 20 analyzed images and representing a surface of approximately 213000 sq km (Fig. 1). The frame scenes were selected in order to include zones with known mining activity of diverse origin (volcanic, metamorphic, and sedimentary) in Central and Eastern Europe.

The area of interest in Poland is Upper Silesia, containing waste from base metals (Zn and Pb) and hard coal. Often, the waste from many closed mines was deposited in landfills together with waste from other industries and/or municipal waste. The region is the most industrialized area of the country and numerous geochemical studies for investigating the soil contamination with heavy metals have been carried out (Lis and Pasiezna 1995a, 1995b, 1995c, 1999a, 1999b in Kasinsky and Gientka, 2004).

The selected area in central Slovakia, covering just over two-thirds of the country's surface area, includes most of the mines (brown coal and lignite, metallic minerals, industrial minerals) and open-pits for construction materials in Slovakia. Since 1990 detailed inventories of existent and old abandoned mining sites have been done, and a system of evaluation and monitoring the mining impacts for selecting the sites to be remedied has been designed and is in implementation phase (Jánová and Vrana, 2004).

The four scenes selected for Romania are located in the regions of Maramureș, Central and Western Transilvania and Northern Oltenia and include mines for bituminous coal, lignite, iron, manganese, copper, base metals (Cu, Pb, Zn), gold, mercury and molybdenum. To these there are added facilities for extracting and processing salt, kaolin, calcite, bentonite, feldspar and talc. Shortly after the beginning of economic restructuring process of the mining sector in the 1990s, provisions for the establishment of a national integrated monitoring system of the environmental quality have been included in the National Environmental Protection Strategy and the National Environmental Action Plan (Veliciu and Stratulat, 2004).

On the whole, the study area is morphologically extremely varied, including plains, plateaus, hills and mountains. The highest peaks are Gerlachovský štít (2654 m) in Tatra Mts. and Pietrosu (2305 m) in the East Carpathians, while the lowest elevations are around 100 m.

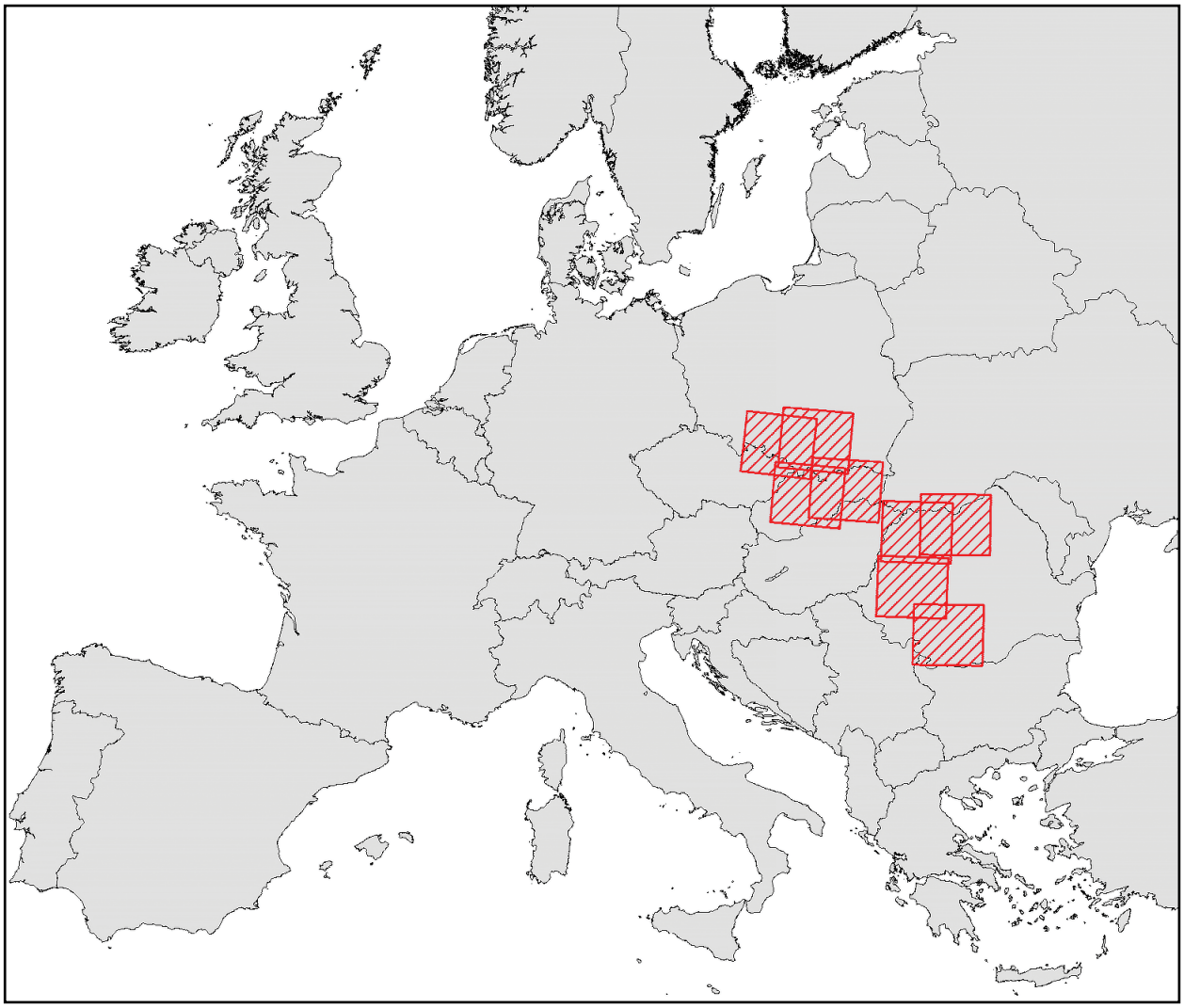

**Fig. 1.** Study area (Landsat TM/ETM frames in Poland, Slovakia, and Romania).

The dense forest cover (coniferous, mixed, and deciduous) is a general characteristic in all three countries. On plains, hills and plateaus, between forests patches of various sizes, arable lands alternate with pastures, grasslands, orchards and to a lesser extent vineyards. The climate is temperate continental with warm and dry summers, while the winters are usually wet and cold.

### 2.2. Data

The processed remote sensing data consisted in Landsat TM and ETM images, dated 1985 to 2000. While the main bulk of the more recent images originate from the IMAGE2000 database of the Institute of Environment and Sustainability of the Joint Research Centre, others were especially acquired within the framework of Pecomines1 project. For checking the remote sensing anomalies we used all data and information made available by our partners in the Steering Committee of the Pecomines1 project (Table 1).

## 3. METHOD

### 3.1. Mapping mining material with Landsat TM /ETM

Numerous laboratory spectral libraries of minerals and rocks have been built since the 1970s (Hunt and Salisbury, 1970, 1971, 1976a, 1976b; Hunt *et al.*, 1971a, 1971b, 1972, 1973a, 1973b, 1974a, 1974b), some of them (United States Geological Survey, Jet Propulsion Laboratory etc.) integrated in commercial image processing packages. While there are minerals that present diagnostic spectral features in the laboratory, rocks, which are an aggregation of minerals, can only be inferred indirectly by detecting spectral features. In most cases they are caused by hydroxyl, carbonate, water and borate vibrational overtones and combination tones, or by electronic transitions in metallic cations. Often the dominant features belong to an accessory mineral or impurity (Hunt, 1980).

In the mining activity, the useful mineral is almost always associated with other minerals, which occur in much more significant quantities.

**Table 1.** Data types used for verification of the remote sensing anomalies

| Data description | Original format | Scale or resolution | Source |
|---|---|---|---|
| mining sites | GIS | 1:50,000 | Institute for Ecology of the Industrial Areas in Poland (IETU – PL) |
| | GIS | 1:50,000<br>1:10,000 | Ministry of Environment of Slovak Republic (ME – SK) |
| | paper | 1:50,000 | Geological Institute of Romania (IGR – RO) |
| open pits | GIS | 1:50,000<br>1:10,000 | ME - SK |
| landfills | GIS | 1:50,000 | IETU – PL |
| old mining dumps | GIS | 1:50,000<br>1:10,000 | ME - SK |
| potential contaminated sites | GIS | 1:50,000 | IETU – PL |
| geology | GIS | 1:50,000 | Polish Geological Institute (PGI – PL) |
| | paper | 1:200,000<br>1:50,000 | IGR - RO |
| | paper | 1:500,000 | Geological Survey of Slovak Republic (SGUDS – SK) |
| hydrogeology | GIS | 1:50,000 | PGI - PL |
| metallogeny | paper | 1:200,000 | IGR - RO |
| mineral resources | paper | 1:1,000,000<br>1:200,000 | IGR - RO |
| soil | paper | 1:1,000,000 | IGR - RO |
| topography | paper | 1:50,000 | National Mapping Agencies in SK and RO |
| CORINE Land Cover | GIS | 100 m | European Environment Agency (EEA) |
| Catchment Characterization and Modeling database (CCM) | GIS | 250 m | Database of the European Commission |

For example, in the case of sulphide ores (Cu, Zn, Pb etc.), pyrite is always prevalent and gives birth to secondary minerals (oxides, hydroxides, hydrated sulphates etc.) by weathering. Another source for their origin can be direct precipitation from the water transporting the soluble metallic ions (Swayze *et al.*, 1996). While pyrite and most other sulphides are generally opaque and have low reflectance values, the secondary minerals (jarosite, ferrihydrite, goethite, hematite, and limonite) have higher reflectance values and some distinct features caused by the iron ion (Fig. 2). These features can be large absorptions between 0.7 and 1 mm (like in jarosite, limonite) or steep falloff of the reflectance towards the blue region (like in hematite, goethite, jarosite, ferrihydrite). Furthermore, there are absorption features due to hydroxyl or water (such as in jarosite, ferrihydrite, limonite Fig. 2) in the infrared region corresponding to Landsat TM band 7.

The areas with accumulations of mineral deposits of hydrothermal origin are usually characterized by haloes of alteration of different degrees, leading to the formation of secondary minerals, some of them exhibiting more or less intense absorptions features in TM7 band, due to metal-OH vibrations bonds (Fig. 3). These minerals also present absorptions due to iron of various intensities or falloff of reflectance in the visible range, depending on the level of the Al and Mg substitution by Fe. Consequently, the waste generated by mined hydrothermal deposits can be identified with Landsat TM imagery based on the specific spectral features caused by a combination of iron oxy-hydroxides and OH-bearing secondary alteration minerals.

In a vast majority of cases, it is possible to distinguish between assemblages of weathering and secondary alteration products that make up the crust of deposited mined material and bare agricultural fields by applying specific image processing techniques, even to imagery with medium spectral resolution such as provided by the Landsat Thematic Mapper sensor. An average soil spectrum made up of 25 spectra available in ENVI 4.3 image processing system from John Hopkins University Spectral Library shows differences from the spectra of secondary alteration minerals (Fig. 3) and also from the spectra of pyrite weathering products (Fig. 2). Sometimes it can be closer in the visible range to some of the iron oxides and hydroxides, generating in these cases a similar spectral response which needs to be filtered out.

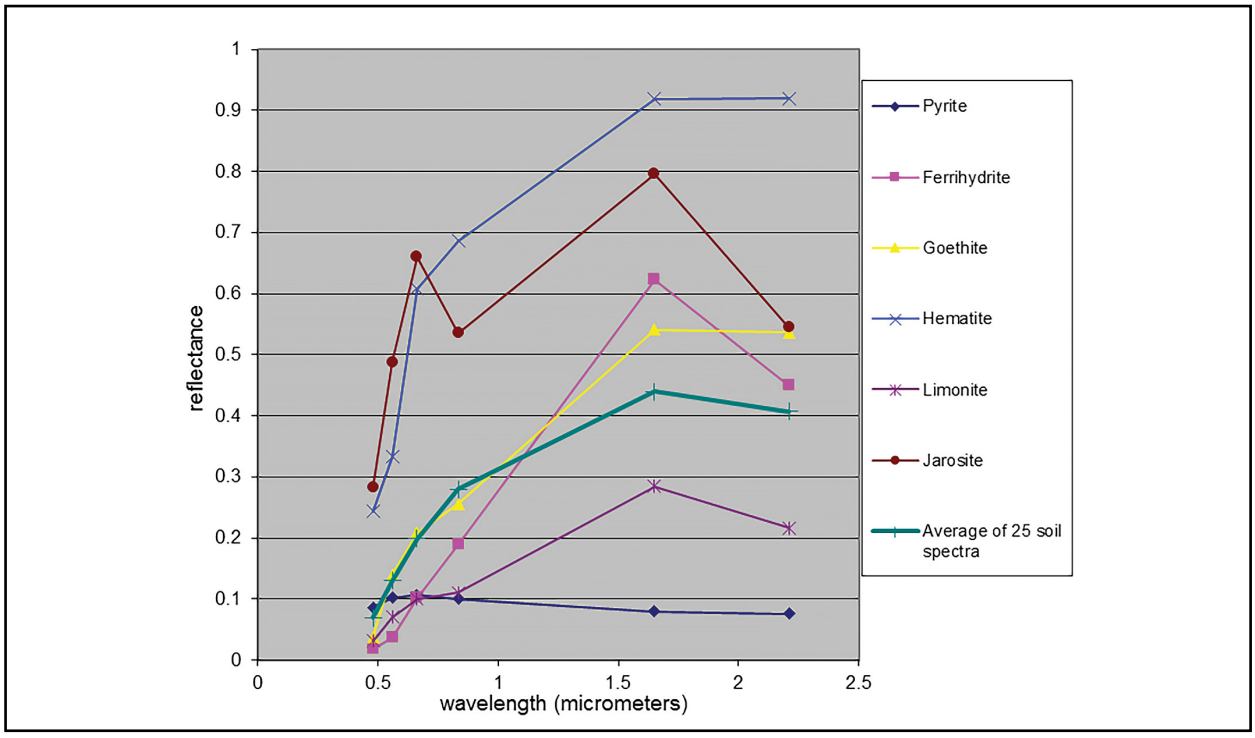


**Fig. 2.** Reflectance spectra of pyrite and the products of its weathering in the Landsat TM spectra (ENVI USGS spectral library).

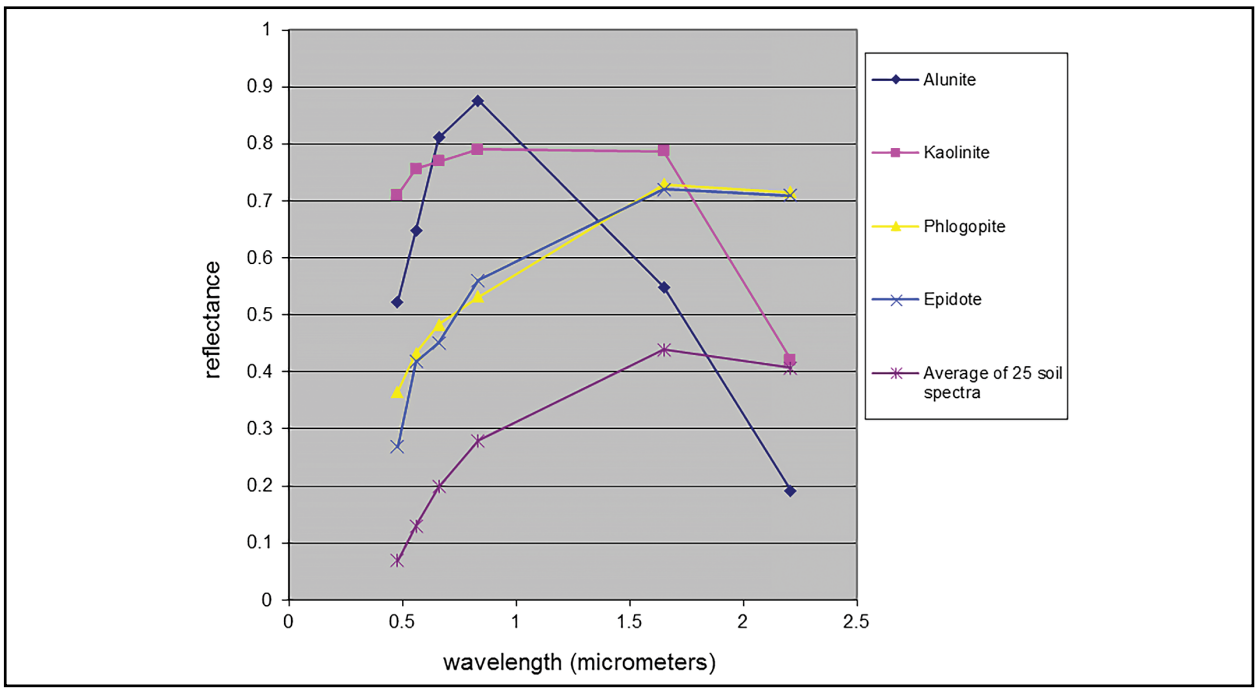


**Fig. 3.** Reflectance spectra of secondary alteration minerals in the Landsat TM spectra (ENVI USGS spectral library).

A great variety of environments contain pyrite distributed in large amounts as an accessory mineral. It can also be found in coal beds and when exposed by mining, comes into contact with water and oxygen, thus generating weathering products and acid mine drainage. This situation is like that of sulphide ore deposits.

There are cases where pyrite is not associated with mineral ore deposits (for example, iron, manganese and magnesium carbonates: siderite, rhodochrosite and magnesite in Fig. 4). By weathering and other reactions of associated minerals, limonite and hematite (for siderite), psilomelan and pyrolusite (for rhodochrosite) and brucite (for magnesite) are generally produced.

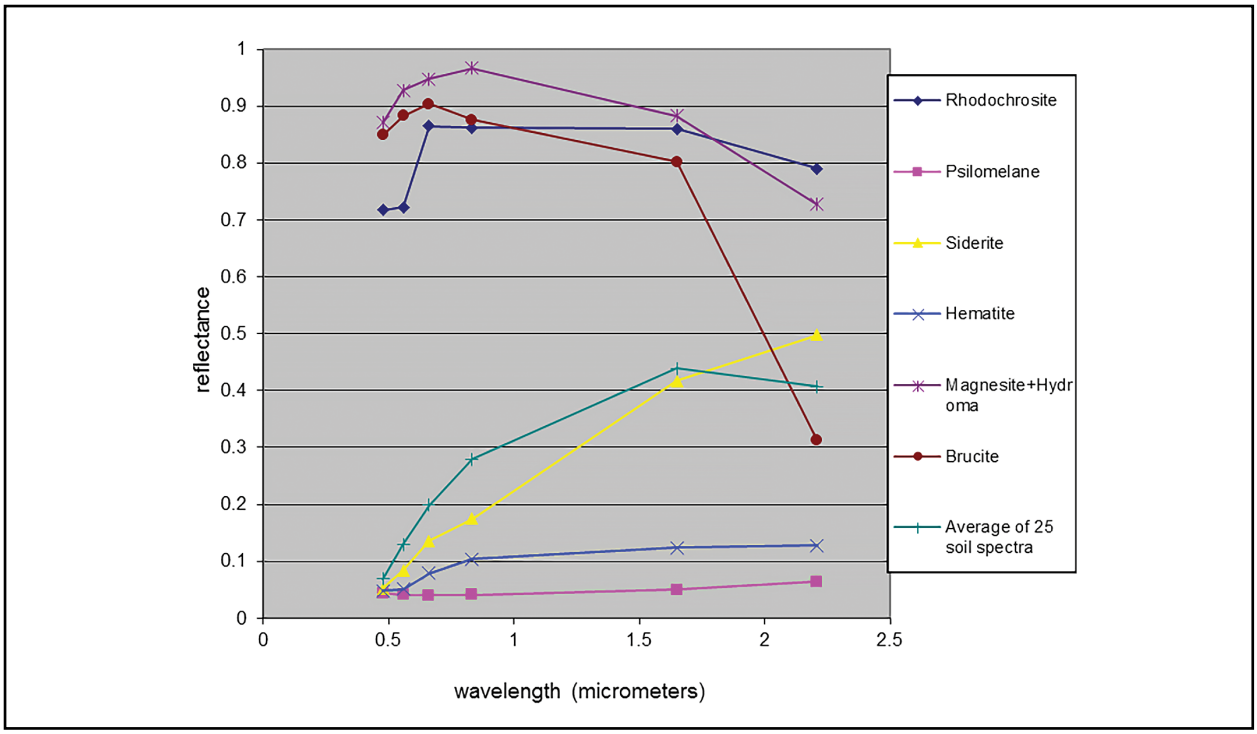


**Fig. 4.** Reflectance spectra of Fe, Mn and Mg ore minerals and weathering products in the Landsat TM spectra (ENVI USGS spectral library).

The waste from these mined deposits can be mapped on Landsat TM images due to the spectral features in the visible wavelengths of the Fe and Mn ions (siderite and rhodochrosite), or high reflectance combined with the specific carbonate bands at wavelenghs longer than 2.0 μm (for magnesite and occurring often in brucite, as a contamination with the former – Hunt *et al.*, 1971a). In this case it is worthwhile noting the difference between the average soil spectrum and the spectra of ores and weathering products.

Mapping mining wastes at a regional scale by means of Landsat TM requires differentiating between the material having a higher reflectance and more pronounced spectral features in the visible and infrared than common soil types and those with a lower reflectance and subtle features, characteristic of many opaque compounds formed by processing coal and metallic ores. Nested between these two situations is the general spectral response of soil. Where local particularities (i.e. enrichment in iron oxides and clay minerals) are present, solutions should be found with image processing techniques for distinguishing between these particular soil types and mining material.

A screening of mining waste material at regional scale requires achieving a compromise between the sizes of the area covered, remote sensing data availability, work costs, processing speed and ground truth data availability. Hyperspectral remote sensing is, as an example, unsuitable for country-wide coverage and the complex processing methods (i.e. feature mapping/absorption maps, full spectral mapping), require sophisticated procedures and a concrete knowledge of the field sites and spectroscopy. Mixture modeling methods, as another example, are also difficult to implement because they are fitted when the surface is dominated by few spectrally distinct components that exhibit continuous changes in relative mixing ratios across the scene. As a compromise, Thematic Mapper data that is processed with a statistical-based method such as Principal Components Analysis (PCA) can be applied in a relatively straightforward manner and is very effective for the identification of regional similarities and differences in surface spectral properties (Mustard and Sunshine in Rencz, 1999).

In this paper we used a PCA-based variant, namely FPCS (Feature-Oriented Principal Component Selection), initially proposed by Crosta and McMoore (1989) and later developed and modified by Loughlin (1990, 1991). By subsetting the total number of spectral channels in order to maximize the variance due to a set of absorption features, a spectral basis is assigned to the simple statistical transform. We first applied the method as modified by Louglin (1991) on atmospherically and geometrically corrected Landsat TM/ETM scenes and subsequently adapt it for use in an operational mode (Fig. 5). The advantages consisted in: **i**) the possibility of applying the same methodology to scenes acquired in different regions and during different seasons; **ii**) the possibility to derive filters based on reflectance values for filtering out non-mining related anomalies, caused by the broad spectral and spatial resolution of TM/ETM data.

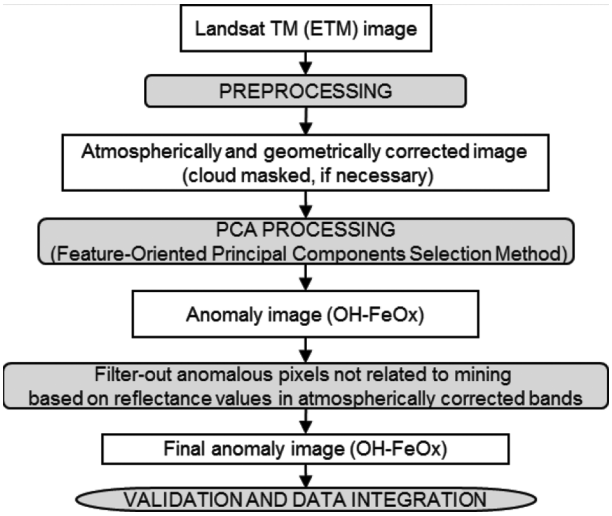


**Fig. 5.** Processing chain of Landsat-TM (ETM) scenes, proposed for a pan-European scale operational mode.

### 3.2. Image preprocessing

The preprocessing consists in radiometric corrections, geometric corrections and applying a cloud mask when necessary. The radiometric corrections implied correcting the signal for the "at-satellite radiance" and for the atmosphere-induced effects based on a modified 5S model "Simulation of Satellite Signal in the Solar Spectrum" created by Tanré *et al.* (1990) with later improvements (Hill, 1993; Lacaze *et al.*, 1996; Hill and Mehl, 2003). It was not possible to compensate the obtained estimated ground reflectances for the topographic effects too, since no digital elevation model of a satisfactory spatial resolution, compatible to Landsat imagery, was available at the time of processing the scenes.

The geometric correction of the Landsat images was implemented using a program whose advantage lies in speeding up the tedious routine work of ground point recognition and selection by a factor of six. It employs a procedure for selecting the ground control points (GCPs) in a semi-automated manner based on three initial GCPs and the cross-correlation computed between the image to be corrected and a reference image at selected roughly estimated coordinates (Hill and Mehl, 2003). This way more than 100 GCPs were obtained for each of the investigated Landsat-TM scenes, the final root mean square (RMS) of the applied polynomial order 2 transformation being less than 0.3 pixels.

A cloud mask was sometimes necessary since the clouds are also mapped in the principal components of interest because of their difference in reflectance in the band pairs TM1-TM3 and TM5-TM7, and thus appear as anomalies. The clouds should therefore be masked as no-data values and excluded from the image statistics prior to running the PCA-based method. An algorithm capable of perfectly masking all types of clouds, including very thin and transparent ones, is not yet known in the remote sensing literature. In the situations where it was needed, a cloud mask was tested using a combination of Normalized Difference Vegetation Index (NDVI) and TM6. The results were good for dense clouds.

Similar results were obtained with a cloud mask made by thresholding one of the principal component images (using the bands 1,4,5,7 for mapping the hydroxyl features), selected by its highest loading in TM1. However, neither method was able to mask the very thin clouds. The remaining cloud-induced anomalies were eliminated in a later phase of validation and data integration.

### 3.3. Mapping mining wastes by operating Principal Components

The method takes over the development introduced by Louglin to the method of "Feature-Oriented Principal Components Selection - FPCS" proposed by Crosta and McMoore (1989), for the purpose of obtaining one single PC-image for FeOx and one PC-image for OH-bearing minerals. This implies performing one PCA on the TM bands where FeOx minerals have diagnostic features (1, 3, 4, and 5) and avoiding TM7 where OH-bearing minerals show absorption features. A second PCA was applied using TM bands (1, 4, 5, and 7) and avoiding TM3 (Fig. 6).

The principal components (PCs) which yielded the FeOx-image and OH-image were selected on the basis of the eigenvectors matrix using the criteria introduced by Loughlin (1991). For mapping iron oxides the pair TM1-TM3 was examined looking for the high or moderate magnitudes in both and opposite sign. The sign of the respective eigenvector in TM3 determined whether or not the iron oxides would be distinguished on the image as bright or dark pixels. If the sign was positive, the iron oxides formed the brightest areas on the image, as there is a raise in reflectance in TM3 compared to TM1. If the sign was negative, the image had to be negated.

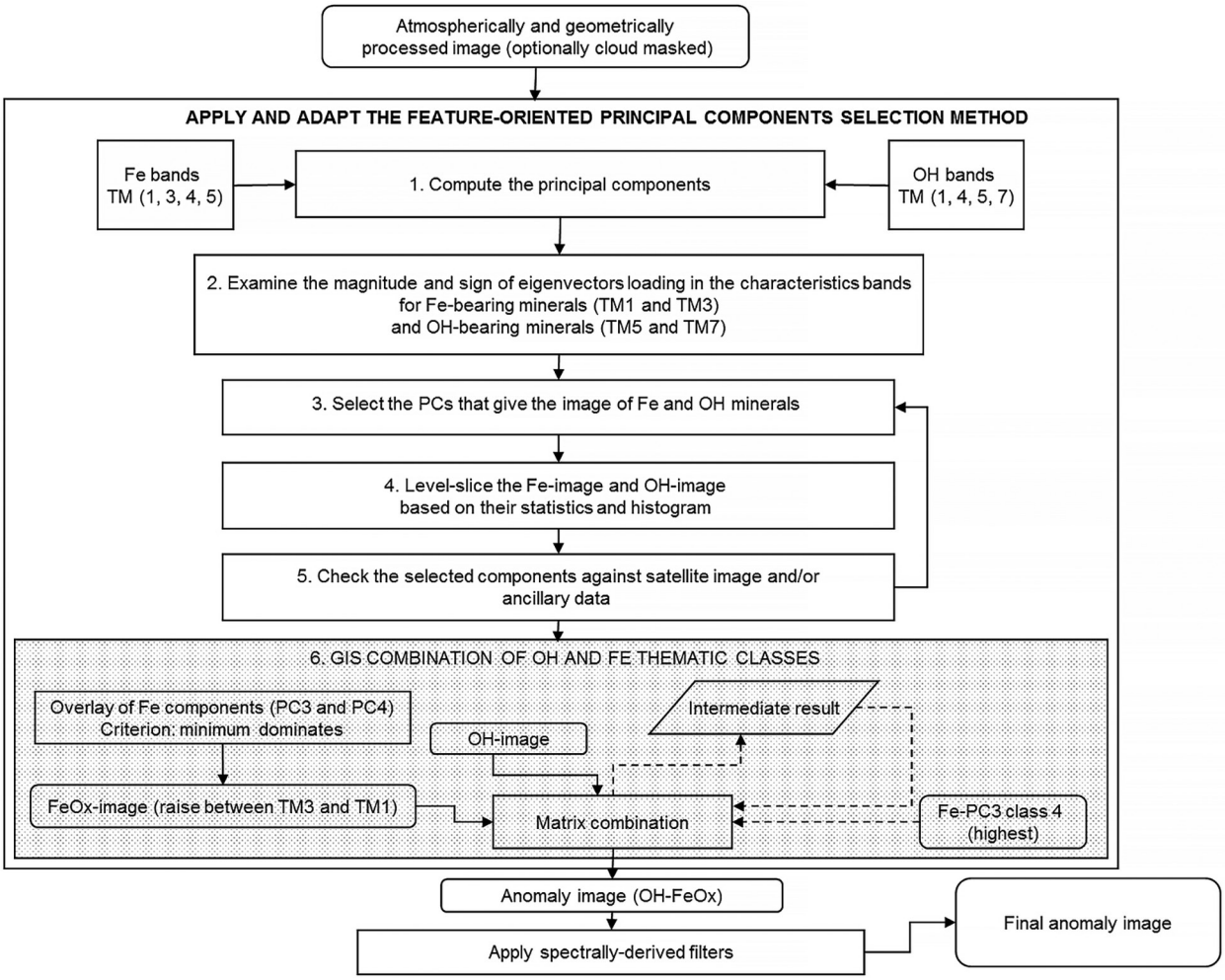


**Fig. 6.** Processing chain for the OH-FeOx anomaly image.

For the image of OH-bearing minerals the TM5-TM7 pair was examined and the selected PC was the one having highest loadings and opposite signs in these bands. The sign of the loading in TM7 was fundamental to the brightness of the areas rich in these minerals because it showed the absorption in TM7 compared to TM5. If the sign was negative, it means that the materials having this absorption band in TM7 and greater reflectance in TM5 would appear on the image as bright pixels. If the contribution of TM7 was positive, then the image should have been negated.

Steps 1 to 3 in the processing chain depicted in figure 6 were followed according to Louglin (1991). Our modifications started from step 4 onward, by transforming the selected PC-image to a thematic layer. Four classes were assigned to the Fe-PC4 (Fig. 7): 1 – low, 2 – medium low, 3 – medium high, 4 – high.

The verification (step 5) of the level-sliced PC4-image of Fe for the first test image (scene 185/27 dated 09.08.1998) showed a good mapping of known mining-related features (open pits, tailing ponds, waste rocks, even very small ones from underground mining, ore processing plants), all these being highlighted by the class richest in iron oxides (class 4). However, maximum values were also shown in grassland areas, alpine pastures and many bare fields in agricultural land. The significant loading of TM4 in PC1 (Table 2) led to the idea that the vegetation is expressed as bright pixels in PC1, which is also responsible for the overall albedo. This is indeed the case for forest, which covers a big part of the above-mentioned satellite scene. As some classes of vegetated pixels were mapped into the selected Fe PC4, it was necessary to remove the non-mining-related anomalies.

In the covariance matrix of eigenvectors, PC3 was selected due to the high loadings of both TM1 and TM3 although the sign was identical. Negated similarly to Fe-PC4, this component highlighted the same mining-related features and showed the grasslands and alpine pasture as minima, being little sensitive to the bare agricultural fields. Instead, turbid water (and when present, clouds, smoke) were shown as maximum due to their higher reflectance in TM1.

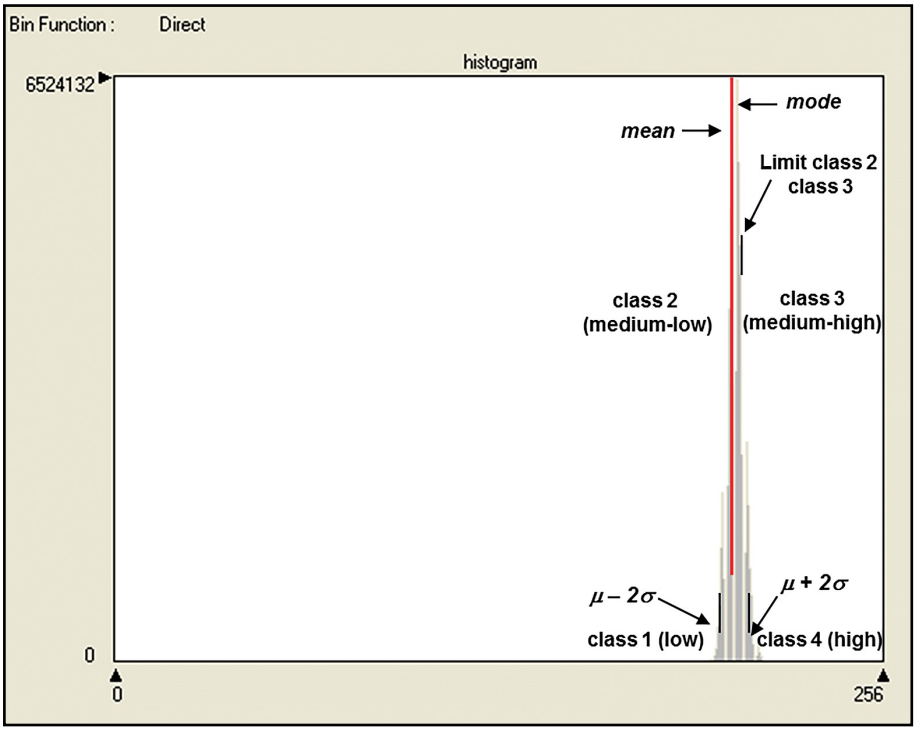


**Fig. 7.** Level-slicing of Fe PC-images based on mean, standard deviation and histogram.

**Table 2.** Covariance eigenvectors for TM bands 1, 3, 4, 5 (Landsat-TM image 185/27)

| | TM1 | TM3 | TM4 | TM5 | Eigenvalue | Variance (%) |
|---|---|---|---|---|---|---|
| PC1 | 0.131 | 0.149 | 0.816 | 0.543 | 4004.41 | 93.34 |
| PC2 | 0.307 | 0.454 | -0.551 | 0.630 | 238.96 | 5.57 |
| PC3 | -0.670 | -0.487 | -0.161 | 0.537 | 41.57 | 0.97 |
| PC4 | 0.663 | -0.732 | -0.068 | 0.143 | 5.32 | 0.12 |
| | | | | | **4290.26** | **100.00** |

By overlaying the level-sliced components Fe-PC3 and Fe-PC4 using the minimum class as criterion (step 6), the pixels classified as being anomalous in grassland and pastures and most of turbid water were removed successfully. The resulting image shows the areas where both iron PCs are the highest as being the brightest pixels and was subsequently input into a matrix combination together with the OH-image that was obtained from PC4 of TM bands 1, 4, 5, 7 (Table 3).

The OH-image classification was sliced into 5 categories, the first three in an identical way with those used for the Fe-PCs. The last two levels represent a further differentiation of the brightest pixels:

- a first group consisting of 2-3 series of brightness values with higher frequency distributed immediately after the limit μ + 2σ (class 4);
- the rest of the pixels with higher brightness values but lower frequencies, more largely distributed up to the value of 255 (class 5). Their cumulated frequency is greater than that of class 4.

**Table 3.** Covariance eigenvectors for TM bands 1, 4, 5, 7 (Landsat-TM image 185/27)

| | TM1 | TM4 | TM5 | TM7 | Eigenvalue | Variance (%) |
|---|---|---|---|---|---|---|
| PC1 | 0.130 | 0.807 | 0.539 | 0.205 | 4085.19 | 93.46 |
| PC2 | -0.267 | 0.573 | -0.613 | -0.474 | 249.65 | 5.71 |
| PC3 | -0.911 | -0.088 | 0.390 | -0.098 | 30.42 | 0.70 |
| PC4 | -0.285 | 0.115 | -0.426 | 0.851 | 5.72 | 0.13 |
| | | | | | **4370.98** | **100.00** |

This differentiation served as a control measure of anomalies (transition between high OH classes) when analyzing time-series satellite scenes.

The output of the matrix combination was an anomaly image based on a combination of OH-FeOx images, highlighting the zones showing iron staining (characterized by a raise in reflectance in TM3 compared to TM1) with various levels in secondary alteration minerals (containing metal-OH bonds producing absorptions in TM7 relative to TM5). These zones corresponded well with mining-related features from the CORINE Land Cover database (CEC, 1993), national databases or thematic paper maps. Detailed inspection revealed however, that there might be mining dump sites and open-cast mines which were partially or totally omitted as anomalies. The image-derived spectra at these locations showed a flat spectral curve or even a decrease in reflectance in TM3 compared to TM1. These areas corresponded to the highest class in both Fe-PC3 and OH-PC4, but lower classes in Fe-PC4. Therefore, a subsequent matrix combination was done using as inputs the OH-FeOx above-mentioned anomaly image and class 4 of Fe-PC3. It resulted an anomaly image with 20 classes of interest (legend on Fig. 8) representing the combination of the highest class (Fe-PC3) with all classes of Fe-PC4 and OH-PC4. From these results, classes 1 to 8 mainly represent oxidation and are poor in OH, while the classes of interest for the topic of mining waste are those rich in OH and rich in iron (Fe-PC3), with different levels of iron staining (Fe-PC4), i.e. classes 13 to 20.

A better mapping of mining-related features was obtained this way as assessed both visually by cross checking against ancillary data and by statistical computation of the anomalous pixels corresponding to known mining objects (open-cast mines, waste rocks, dump sites, tailing ponds etc.). Figure 8 presents an example of the visual check performed where the image-derived spectra on Landsat-TM 185/28 dated 25.09.1992 at three locations situated inside the porphyry-copper opencast mine of Roșia Poieni, (spectra 1, 2 and 4) and on its associated tailings pond Valea Șesii (spectrum 3) in the Apuseni Mts., Romania, are shown.

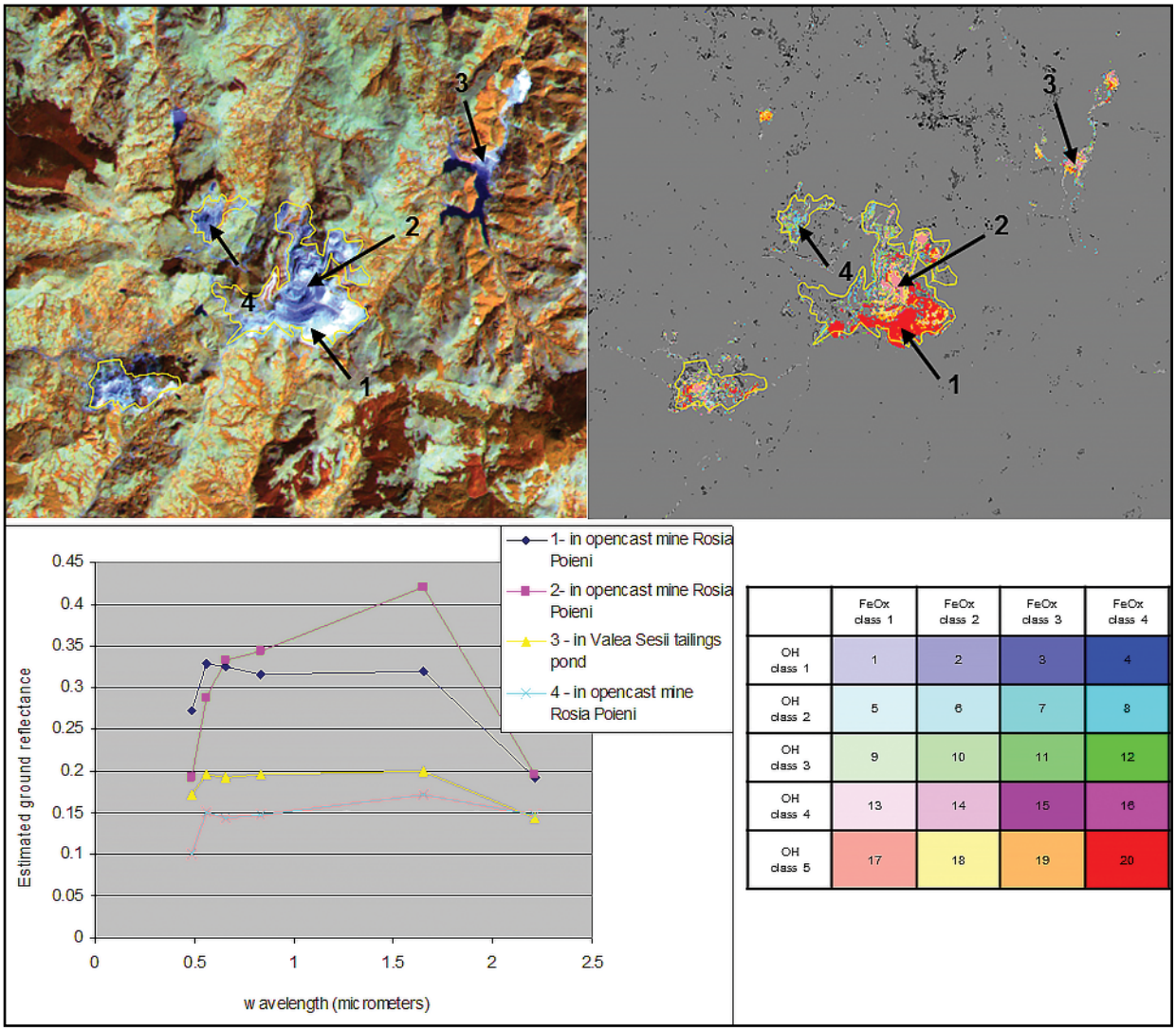


**Fig. 8.** Image-derived spectra (Apuseni Mts., Romania), showing the difference in highlighting mining-related features between the two Fe PCs. Yellow polygons on the image represent mineral extraction sites (CLC database).

This mine is recognized by the national authorities in Romania for its acidification problems (Veliciu and Stratulat, 2004). In the intermediate anomaly image only spectrum 2 corresponds to OH-FeOx anomalies (maximum in both Fe PCs). Spectra no. 1, 3 and 4 show large absorptions in TM3 that extend up to 1.5 µm and can also occur in mining material (pointed out by maximum in Fe PC3).

### 3.4. Filtering anomalous pixels

The best possible mapping of mining material by a simple and straightforward procedure implying operations with selected PCs of Landsat TM (ETM) bands was achieved so far after performing step 6 (Fig. 6). The rather wide spectral bandwidths of Thematic Mapper determined that in the selected Fe and OH PCs, some pixels that are not mining-related were also mapped in a similar way to mining material. Such pixels represent mainly bare soils on agricultural land and turbid/eutrophic water and most of them have been reintroduced by the combination with Fe-PC3 (class 4).

Some filters were created to reduce these anomalies without affecting the anomalies in mining objects. These filters were developed based on reflectance values in atmospherically corrected TM (ETM) bands for turbid/eutrophic water and for soil.

#### *3.4.1. Filtering anomalous pixels in turbid/eutrophic water*

The approach for filtering out the anomalous pixels in turbid/eutrophic water was to identify all water bodies/courses and then to exclude them from the desired class representing turbid water with suspended minerals in the tailing ponds. It did not matter that water bodies and rivers that were not highlighted by anomalous pixels were also set to zero. To map all water bodies, the reflectance values in TM5 and TM1 were exploited by stretching the 0-255 digital number scale to a range from 0-100%.

The pixels having TM5 <= 5% reflectance (13DN) and TM1 >= 1% (3DN) were selected, the latter in order to exclude shadowed pixels on deep slopes. From this group of pixels, we excluded those having TM3 >= 10% (26 DN). These conditions were satisfactory for efficiently filtering out most of the anomalous pixels in water (Fig. 9) and maintaining the water with suspended minerals characteristic for tailing ponds.

#### *3.4.2. Filtering anomalous pixels on agricultural fields*

Agricultural land can generate a number of anomalous pixels that generally represent a small proportion of the entire agricultural surface in one satellite scene: a couple of percentage points according to statistical analysis for Poland, Slovakia and Romania. However, there are cases when these anomalies can cover a whole parcel, being similar or even greater (when summed up) than the anomalies highlighting mining-related features (small dumps or waste rock piles, tiny tailing ponds) and therefore need to be filtered out.

We analyzed the distribution of anomalous pixels in agricultural land using the CORINE LC database as a reference and separating three categories based on NDVI values within it:

- Predominant bare soils NDVI <= 0.15
- Mixtures soil-vegetation 0.15 < NDVI < 0.5
- Predominant vegetation cover NDVI >= 0.5

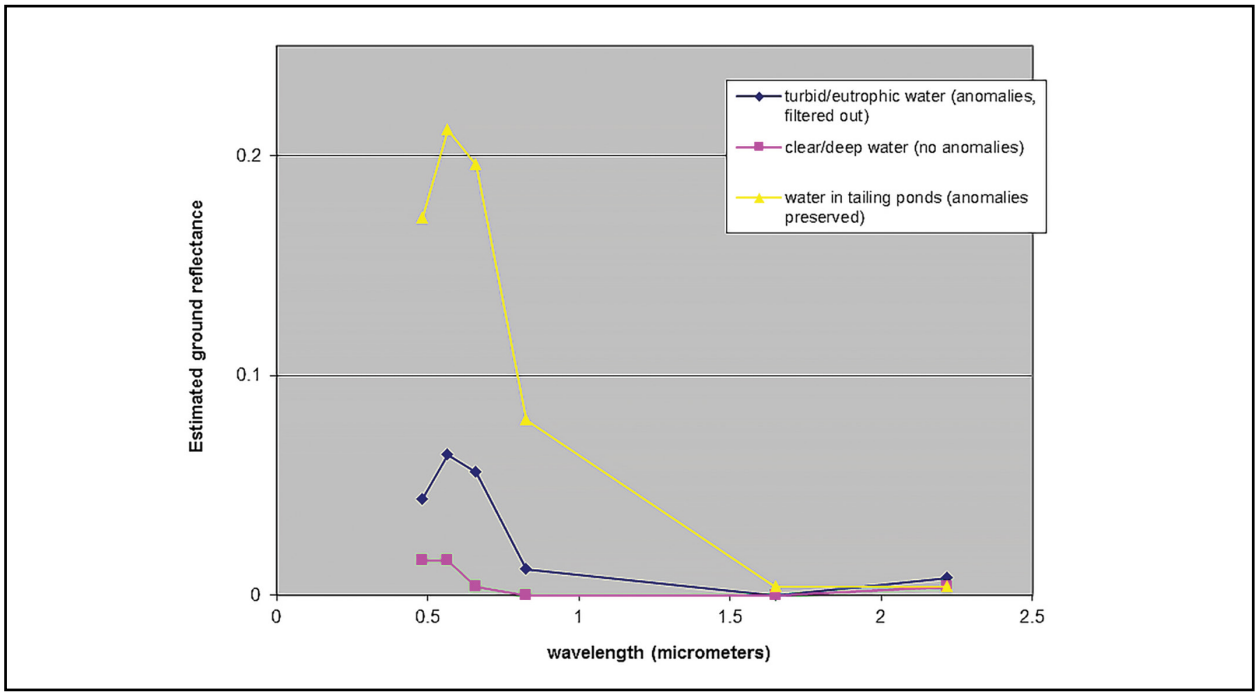


**Fig. 9.** Image-derived spectra for water (ETM 189/25, 14.05.2000) showing the types of features filtered out and preserved.

**Table 4.** Distribution of anomalous pixels before and after filtering

| | | Area (%) | Anomalous pixels (%) | Proportion of area causing anomalies (%) | Proportion of area causing anomalies, after filtering (%) | Relative decrease of anomalous pixels after filtering (%) |
|---|---|---|---|---|---|---|
| **Agriculture** | Predominantly bare | 3.8 | 26.1 | 31.6 | 9.5 | 68.5 |
| | Mixed | 44.5 | 39.4 | 3.4 | 1.8 | 44.1 |
| | Predominantly vegetated | 51.6 | 34.6 | 2.3 | 0 | 0 |
| **Other** | Predominantly bare | 3.2 | 38.9 | 32.5 | 26.4 | 18.5 |
| | Mixed | 15.2 | 50.6 | 8.8 | 8.0 | 12.0 |
| | Predominantly vegetated | 81.6 | 10.4 | 0.3 | 0 | 0 |

Table 4 shows the percentage distribution of anomalies in the above-mentioned categories for agricultural land, as well as for the rest of the land cover classes grouped together as "others" and including mining-related features, artificial surfaces, forests and other natural vegetation areas, water bodies etc., classified only according to the NDVI thresholds. The table refers to average values computed for these two main categories taking into account four satellite scenes: ETM 189/25 (14.05.2000), ETM 188/25 (07.05.2000) covering southern Poland and parts of Czech Republic (Upper Silesia), 184/29 (15.10.1990) and 185/28 (25.09.1992) in South-West and West Romania.

Anomalies on agricultural areas with predominant vegetation cover represent a small percentage of the relative area (2.3%), although, depending on the season, the number of anomalous pixels can be high. These anomalies might be caused by mixed pixels, where the radiance from soil determines a high value in sensor bands 3 and 1 (Fig. 10), while the green plants are responsible for a very high value in the near infrared (band 4). The NDVI of these areas is higher than 0.5 and we filtered out this type of anomaly by applying the threshold. Once more, the fact that other types of vegetation with higher NDVI, such as forests (mapped in the low-order PCs, therefore cause no problems), was set to zero, was of no relevance for our study.

A higher percentage of anomalies are found on predominantly bare soils (31.6%) and, to a lesser extent, on mixtures of soil-vegetation (sparse vegetation – 3.4%). Filtering them out was a more difficult task due to the similar response of soils rich in iron oxides (coupled with rich carbonate or clay content) to the spectral features of some of the host rock of open-cast mines or quarries. A perfect discrimination is impossible to achieve using Landsat TM or ETM exclusively. This filter was designed to compromise between filtering out a maximum number of anomalous pixels on the bare soils, while keeping the high oxidation features (significant raise in TM3 compared to TM1) and the flat spectral features (close values in TM1 and TM3).

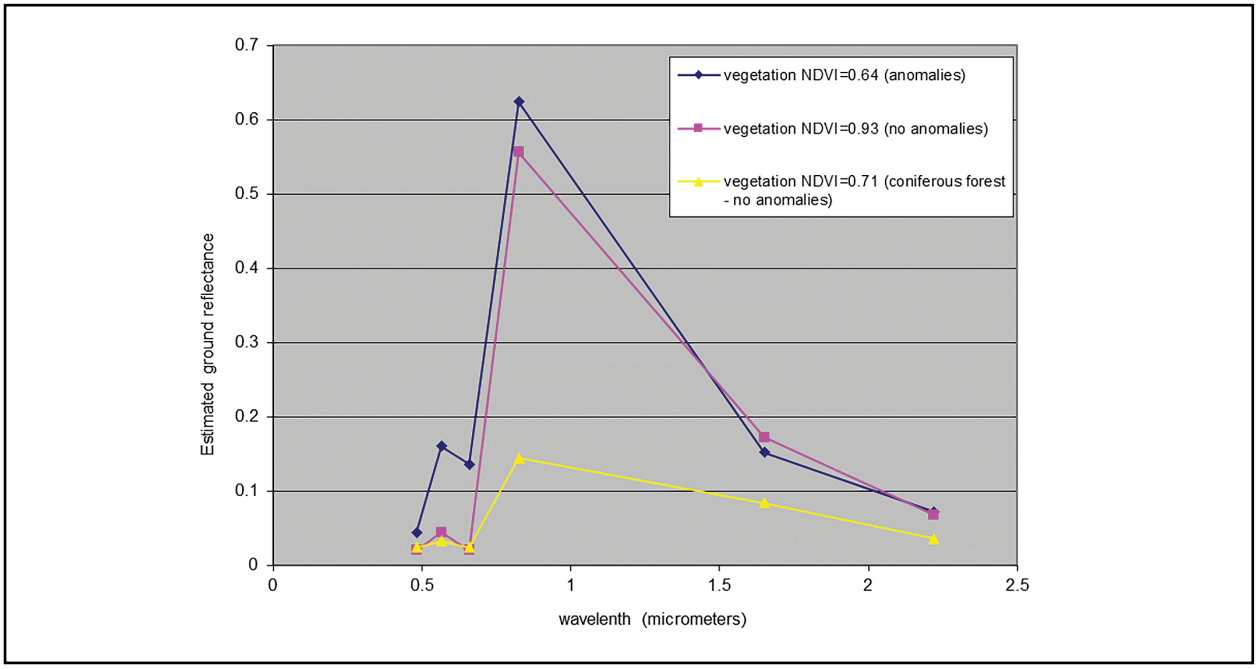


**Fig. 10.** Image-derived spectra of vegetation (ETM 189/25, 14.05.2000) showing the vegetation type filtered out from the OH-FeOx anomaly image.

The following conditions applied: (TM3 – TM1) > 5% reflectance (13 DN) combined with TM1 <= 20% reflectance (52 DN) and applied to the OH-FeOx anomaly classes where the contribution from Fe-PC4 was different from class 4 (the highest). The filter worked well for all the processed scenes (ETM and TM) acquired in different seasons (Fig. 11 and Table 4). The biggest reduction in non-mining related anomalous pixels was indeed for the areas labeled as "predominantly bare soil" and, to a lesser degree, for the "mixed soil-vegetation" areas (table 4). After the filtering process, the greatest proportion of anomalies (relative to the respective area) remained in the category "Other", artificially "predominantly bare" land (where mining-related features are included), followed by the mixed artificial-vegetated areas (Table 4).

## 4. RESULTS AND DISCUSSIONS

### 4.1. Cross-checking with national data sets

The proposed method was tested on 20 multi-temporal scenes consisting mainly of Landsat TM images and some ETM scenes from Central and Eastern Europe. For all analyzed satellite images the sign of OH-PC4 and Fe-PC4 was consistently positive, respectively negative. In three cases, the sign of Fe-PC3 was different from Fe-PC4 (positive instead of negative). In all 20 images, following the criteria of the sign stated in Loughlin (1991) of negating the respective PC-image when necessary, the mining-related features were highlighted as the brightest pixels in the image. The spectrally derived filters worked well on all scenes. From the multi-temporal case studies it was seen that generally the OH-FeOx anomalies occur over time in the same area unless significant change happened (Fig. 12, location 1 – flooding of an open-pit; location 2 – remediation and cover of a dump site by vegetation during a longer time period etc.). The majority class did not always remain the same due to the modifications that take place over time in the surface materials and/or mixtures, as shown in the image-derived spectra.

A reduction of the intensity of OH-FeOx anomalies over time, indicating a decreasing anomaly class and subsequently lower levels of OH-bearing minerals, is observed in the example selected for Upper Silesia (Fig. 12). The area is approximately 15×15 km and contains waste from coal mining, ash from power plant generation, industrial slag and mixtures of various industrial and municipal wastes (Kasinsky *et al.*, 2007). The same tendency was observed as well in other areas with mining activity from Slovakia and Romania.

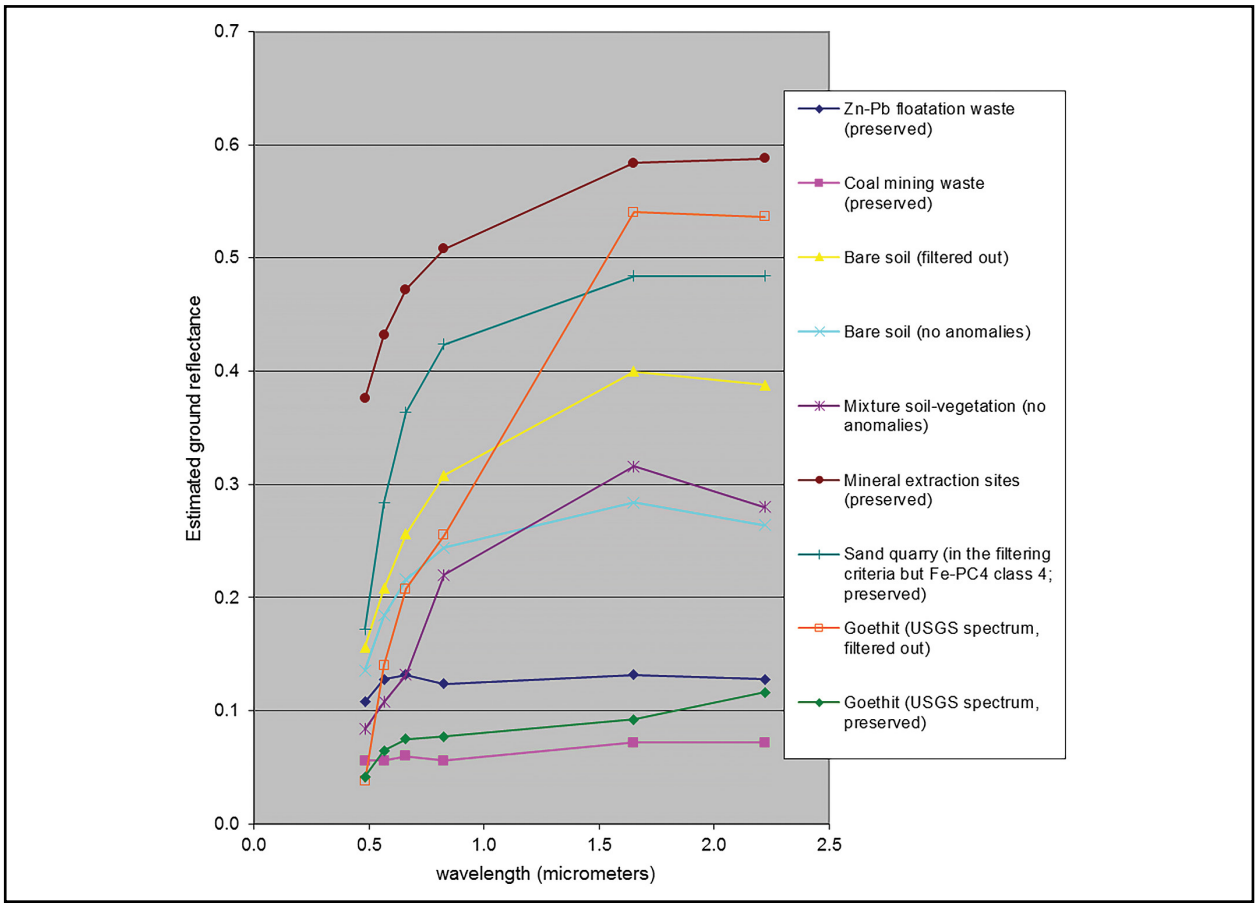


**Fig. 11.** Image-derived spectra of mining wastes and soils (ETM 189/25, 14.05.2000) illustrating the types of spectral features filtered out and preserved.

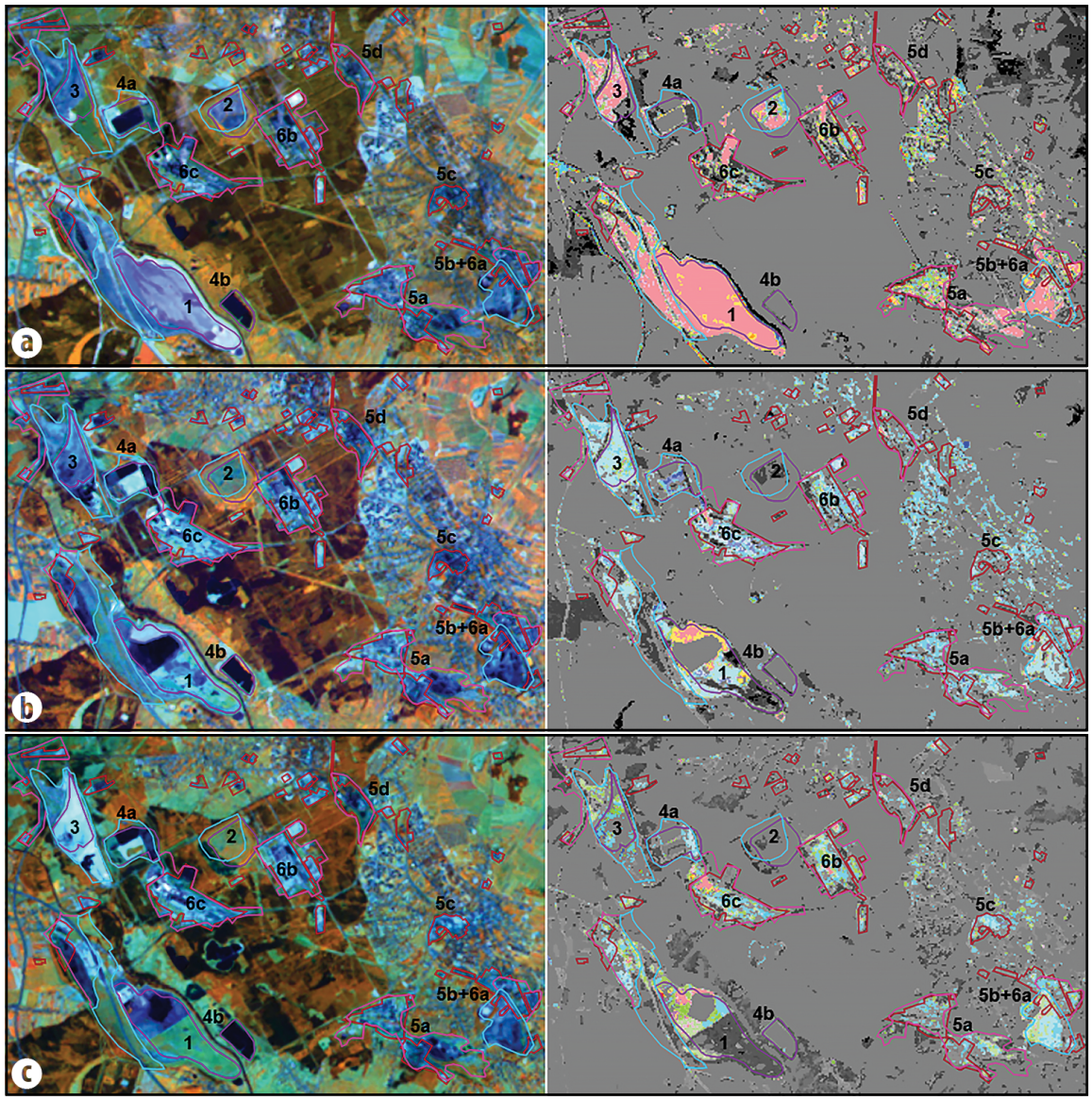


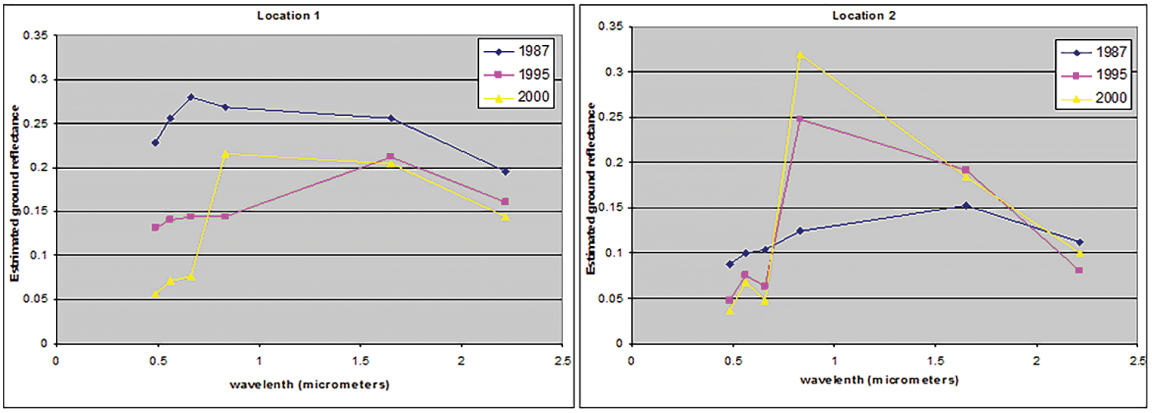


**Fig. 12.** Multi-temporal satellite (*left*) and associated OH-FeOx anomaly images (*right*) in Upper Silesia (Poland), North-East of Katowice. **a**) Landsat-TM (23.08.1987); **b**) Landsat TM (21.07.1995); **c**) Landsat ETM (07.05.2000). CLC 121, CLC 132 – standard nomenclature of CORINE Land Cover classes (CLC). Numeration in the figures correspond to the Polish GIS database of landfills.

This might be explained by the closing of many mines in these regions of Central and East Europe after 1990s, the remediation of the dumps and the introduction of measures for reducing the gaseous/particle emissions of the associated industries.

The cross-checking with mining-related features from the pan-European CORINE Land Cover database or national databases in Poland, Slovakia and Romania, confirmed the applicability of the method by correctly identifying the areas of open-cast mines, open-pits, quarries, dump sites, tailing ponds, smelters and ore processing plants as anomalous pixels. It was also possible to map waste material deposited in the surroundings of underground mines located in forested areas if the exposed surface was at least a couple of Landsat-TM pixels size (Vîjdea *et al.*, 2004). For example, in the Neogene volcanic area of East Carpathians, Baia Mare region (Maramureș county - Romania), the small clusters of anomalous OH-FeOx pixels (Fig. 13) were confirmed by the detailed geological maps (Borcoș *et al.*, 1980) as rock waste piles originated by the underground mines (Pb, Zn, Cu ± Au, Ag) of the Ilba-Băiuț metallogenic district.

Generally, the waste from base metal mines, flotation ponds and their processed tailings, dumps or open-cast mines with acknowledged acidification problems were highlighted as anomalous pixels rich in iron oxides (class 4 Fe-PC3), high in OH (classes 4 or 5) and with various levels of iron staining (materialized by raise in TM3 compared to TM1), which corresponded to various levels in Fe-PC4. The OH-FeOx anomaly classes for these materials are usually 13 to 20 (Fig. 8). In the case of rocks that present absorptions in TM7 compared to TM5 (limestones, dolomites, clays) in their spectra, they are evidenced by high order anomaly classes. The open-pits for extracting sand, gravel and the quarries for building materials are generally highlighted only by the anomaly classes showing mainly oxidation (classes 1 to 8).

### 4.2. Statistical analysis of OH-FeOx anomaly occurrences

#### *4.2.1. Global distribution of OH-FeOx anomalies*

The suitability of the method for mapping mining waste sites and associated industrial sites was demonstrated by the results obtained when computing the statistical distribution of anomalies occurring in various land cover classes.

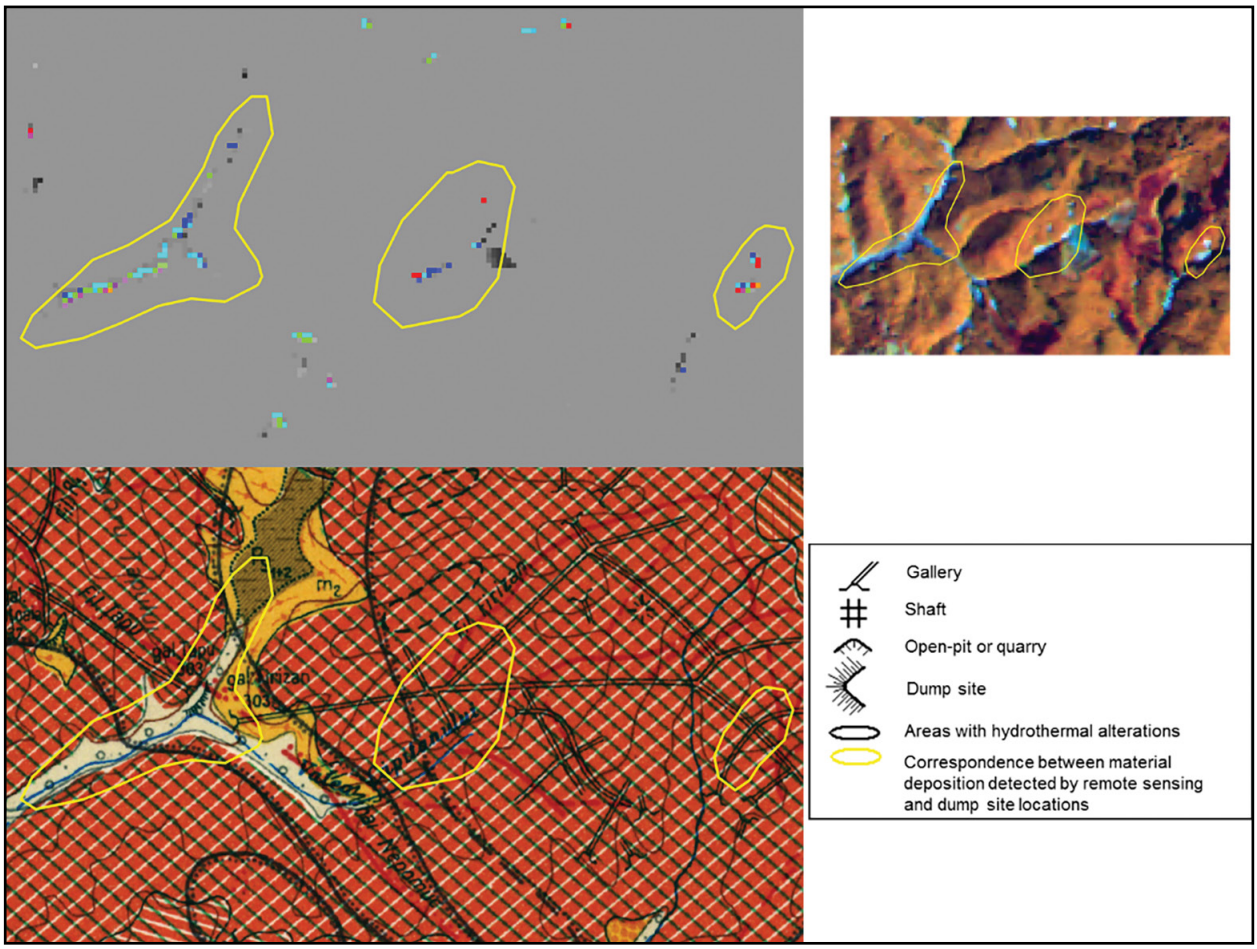


**Fig. 13.** Confirmation of correspondence between anomalous pixels and features related to mining industry by means of 1:50,000 geological map (Borcoș *et al.*, 1980) in the area of Ilba-Handal mine (East Carpathians, Romania).

Figure 14 shows that the mining-related features represented by: **1**) CORINE classes mineral extraction sites, dumps and industrial units (CLC, 1993); **2**) mining wastes sites and potentially contaminated sites from national database (Kasinski *et al.*, 2007); are indeed the classes with the greatest percentage of their area highlighted by anomalous OH-FeOx pixels. We cannot expect to have a 100% correspondence with the surface of the mining-related features, in the way they are delimited in the CORINE Land Cover or national databases, because these features usually include more objects (shafts, tailing ponds, tiny dumps, small processing plants together with surrounding more or less vegetated pixels) into a single entity (polygon). These polygons represent the respective economic unit or several economic units grouped together due to a criterion of minimum size of the mapping unit in various databases (for example, 25 ha in CORINE CLC – CEC, 1993).

After the mining-related features, with a lower percentage of correspondence of anomaly classes (Fig. 14), come the categories of construction sites, transport units (railways, ports and airports facilities) and urban areas - all characterized by cement/asphalt surfaces, metallic roofs/objects, emissions of dust, particles and smoke. Turbid waters and mixtures natural vegetation-soil or vegetation-artificial surfaces have a smaller percentage of anomalies, and the lowest proportion (less than 1%) is found in agricultural areas, forests and areas of scrub and/or herbaceous vegetation associations (grasslands, transitional woodland-scrub, heathlands etc.- CEC, 1993).

The statistical analysis done for Slovakia showed the same trend, the biggest proportion of anomalous OH-FeOx pixels being found in the mining-related CORINE classes mineral extraction sites, dumps sites, industrial units, followed by buffered mines, sites for construction materials and dumps (Fig. 15). Buffers of a 500 meter radius were built around point coordinates of mines (for metallic minerals, coal and industrial minerals) and open-pits for extracting building materials from the Slovak database. The choice of this radius was based on a combination of the Landsat-TM image resolution (30 m, resampled to 25 m after the geometrical correction); the mapping precision of CORINE Land Cover data (100 m); and the minimum area mapping size for the CORINE database (25 ha). By choosing a 20 pixels radius we could ensure an area three times bigger than the minimum mapping unit for the buffered points in order to compensate eventual imprecision of locations between CORINE polygons and the Slovak database. The scope was to identify the correspondence between the two and, in turn, the anomaly OH-FeOx images. The spatial dimension of CORINE polygons was complemented by the more precise extent of deposited material highlighted by the OH-FeOx anomalies, which also gave indications about its very broad geochemical nature (only oxidized or having suffered secondary alteration). Further information such as the mined commodity was attributed by the buffered point.

The good selection of the buffer radius was confirmed by the fact that more than 53% of the summed area of CORINE mineral extraction sites was common to the buffered mining features of the Slovak database. To this the number of hits between the buffered mines and sites for construction materials and the boundaries of the CORINE mineral extraction sites (equivalent to 73 hits for 82 polygons, or 89%) is added (Vîjdea *et al.*, 2004).

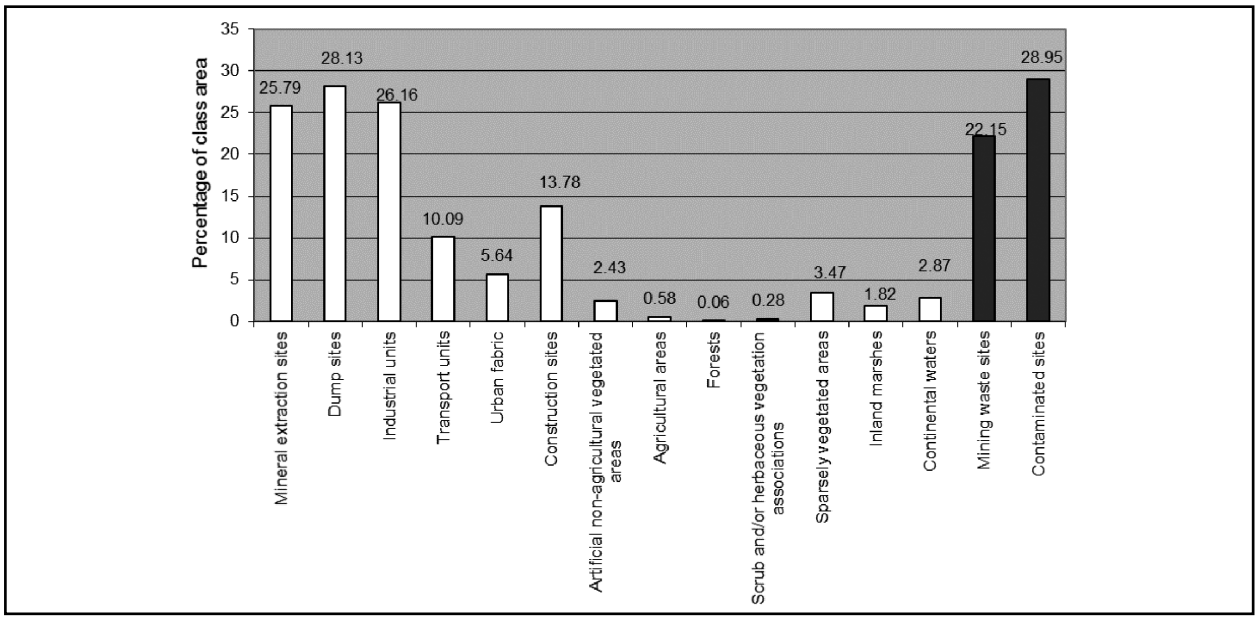


**Fig. 14.** Distribution of total anomalous OH-FeOx pixels in CORINE Land Cover classes and national datasets (mining waste sites and potentially contaminated sites) in Upper Silesia (Poland)

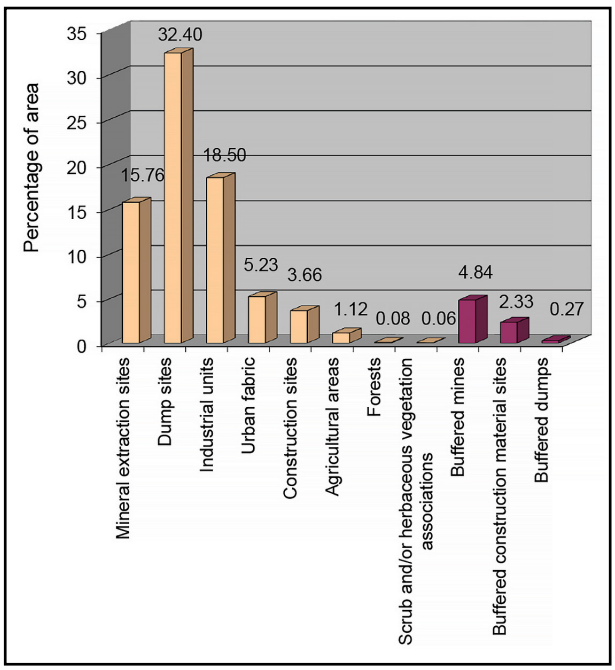


**Fig. 15.** Distribution of total anomalous OH-FeOx pixels in CORINE Land Cover classes and national datasets (buffered mining features) in Slovakia.

A radius of 100 meters was used for buffering the old historical dumps of the Slovak database because these dumps are generally not visible on the images, being located in very dense forest and often below the image resolution (the distance between adjoining points less than 25 m).

### *4.2.2. Differential distribution of OH-FeOx anomalies*

The majority of the Slovak database point mining features (mines, sites for construction materials and old dumps) are located in forests (42.86%, 43.73%, respectively 84.67%) and agricultural areas (37.14%, 40.11%, respectively 10.56%). There is a correspondence of 12.86% of the mines and 11.14% of the sites for construction materials with the CORINE mineral extraction sites. However, the interest was in finding out how many of the anomalous pixels found out in forests, agricultural areas and "areas of scrub and/or herbaceous vegetation associations" (which followed with a distribution of 2.23% for the sites of construction materials and 2.75% for the old dumps) were in reality caused by mining.

The results (Fig. 16) show the highest correspondence values for forest, followed by "areas of scrub and/or herbaceous vegetation associations" and agriculture. Moreover, as we restricted the analysis from all anomaly classes (1 to 20 in the legend of Fig. 8) to the highly anomalous classes (richest in OH-bearing minerals), i.e. classes 13 to 20, and then to the two highest classes (19 and 20) it is seen that the proportions increase. The lowest figures are found for the agricultural areas and this can be explained by the fact that many bare fields are present in this land cover class, some of them having a spectral response in Landsat TM bands similar with the mining material. The filter described in section 3.4.2 substantially reduced these types of anomalies, but it could not eliminate them completely. However, the same pattern of an increase of percentage for highly anomalous classes can be noted too.

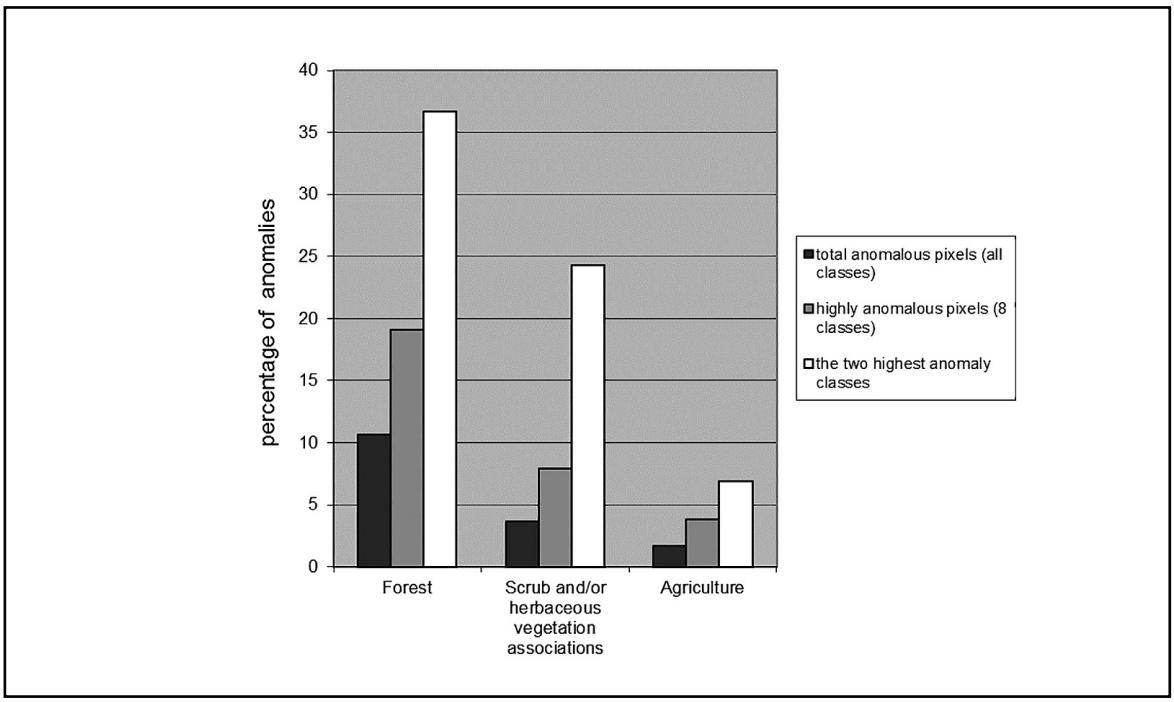


**Fig. 16.** Distribution of anomalous pixels identified in buffered mining features from the Slovak database located in forests, areas of "scrub and/or herbaceous vegetation associations" and agriculture, as percentage of the respective OH-FeOx anomalies in the CORINE class.

The fact that the higher order OH-FeOx anomalies are mostly indicative for mining material is once more demonstrated by the distribution of highly anomalous pixels (classes 13 to 20, Fig. 8) in the main land cover classes of the study area in Slovakia and in the buffered mining features of the Slovak database. The greatest number of these anomalies is found in mineral extraction sites, dumps sites and associated industrial units according to the CORINE land cover database and in buffered point mining features. The results show the same trend when the anomalies were computed both as percentage of the mapped area in the respective land cover class (Fig. 17a), and as percentage of the total anomalous pixels of that class (Fig. 17b).

The OH-FeOx classes representing mainly oxidation (classes 1 to 8, Fig. 8) show the same distribution when computed as percentage of the mapped area of the land cover class (Fig. 18a). This was to be expected and it is normal, as it is one of the starting hypotheses of our method. However, the pattern is changed when the proportion of total anomalous pixels in the respective class are taken into account. A quasi uniform distribution of the simple oxidation anomalies can be noted across all categories (Fig. 18b), with an evident domination in agricultural areas.

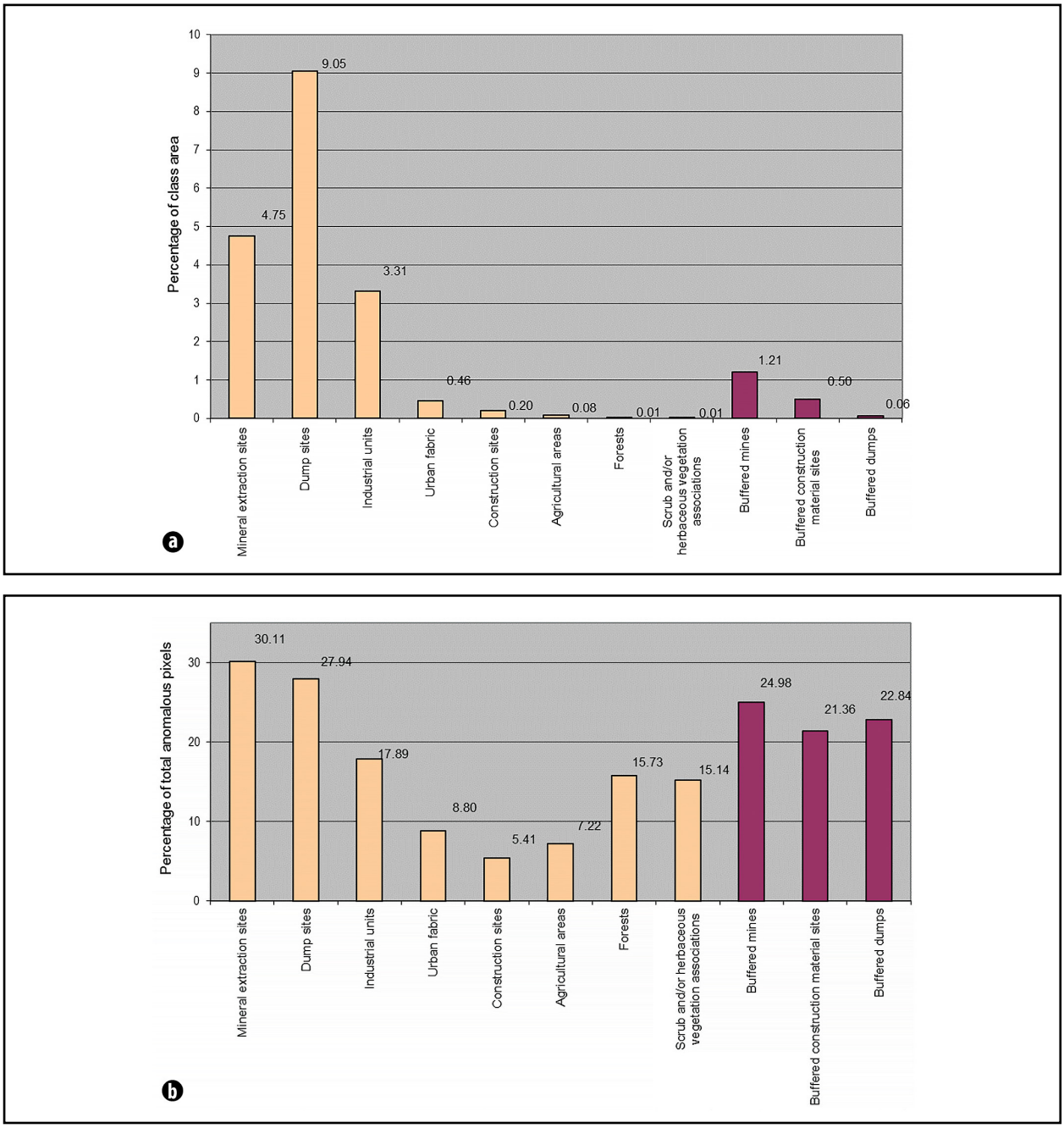


**Fig. 17.** Distribution of highly anomalous pixels (classes 13 to 20) in the main CLC classes and buffered mining features of the Slovak database; **a**) as percentage of class area; **b**) as percentage of total anomalous pixels of the class

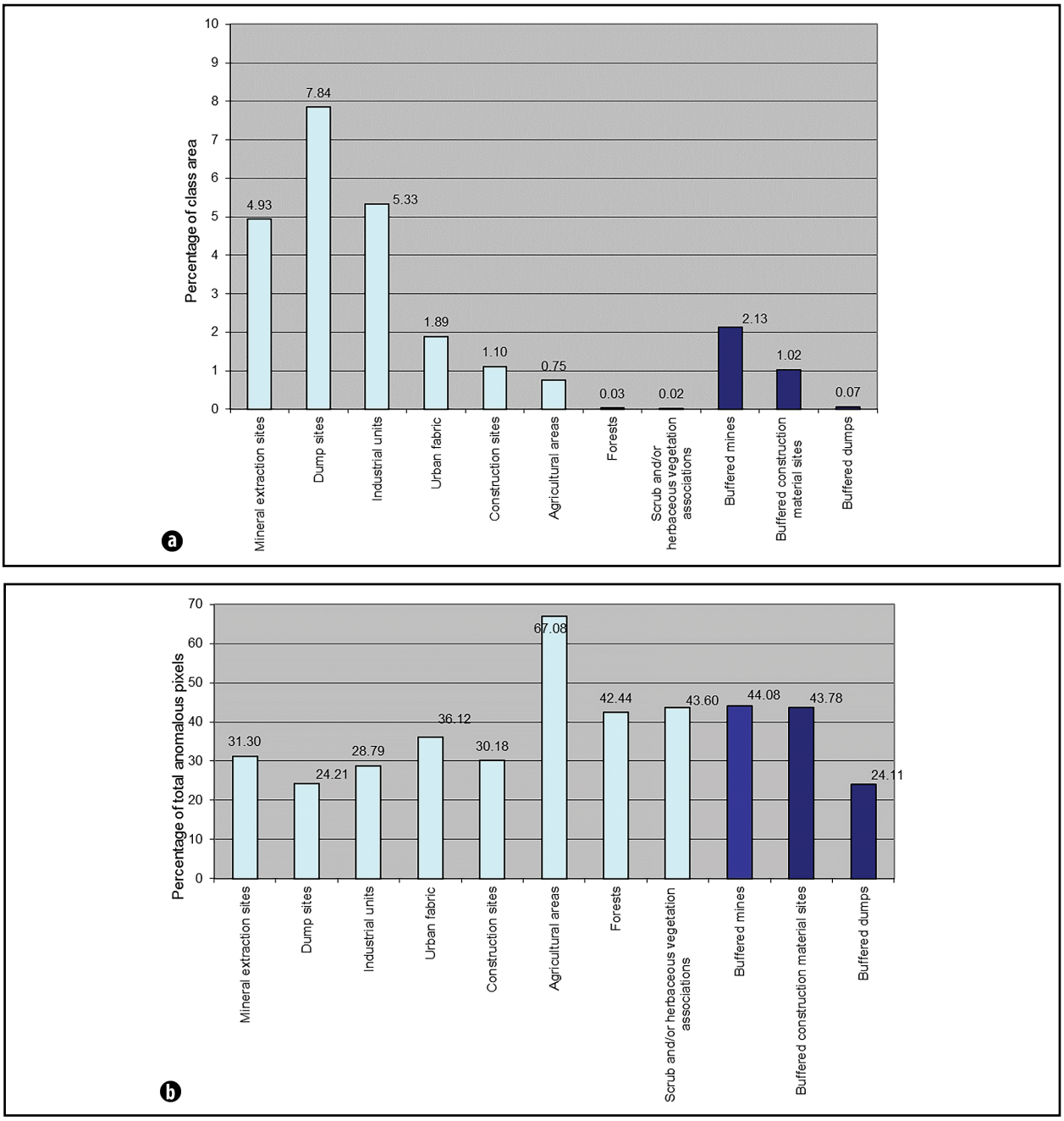


**Fig. 18.** Distribution of simple oxidation anomalous pixels (classes 1 to 8) in the main CLC classes and buffered mining features of the Slovak database; **a**) as percentage of class area; **b**) as percentage of total anomalous pixels of the class.

### *4.2.3. Mining Anomaly Index*

This marked difference in the distribution of OH-FeOx anomaly classes led to the development of an index for a certain type of area reference (catchments, administrative units etc.), which characterize the surface for deposited mining material. The proposed formula for the Mining Anomaly Index (MAI) is:

The MAI is expressed as percentages of the surface of reference (catchments, administrative units etc.) and can output values even greater than 100% if the proportion of highly anomalous pixels within total anomalies is big. When there is no anomaly class between 13 and 20, the index is defined by the percentage of total anomalous pixels, but the value is ten times reduced, thus indicating the presence of less hazardous material.

$$MAI = \left(0.1 + \frac{Number\ of\ highly\ anomalous\ pixels\ (classes\ 13\ to\ 20)}{1 + Number\ of\ mainly\ oxidation\ anomalous\ pixels\ (classes\ 1\ to\ 8)}\right)\left(\frac{Total\ anomalous\ pixels}{Area\ in\ pixels} \times 100\right) \quad (1)$$

An attempt to classify the first order catchments of Slovakia (CCM version 1.2) according to the MAI values led to the following rough scheme:

- (1) MAI <= 0.5 %, corresponding to the background and making up more than 90% of the catchments;
- (2) 0.5 < MAI <= 1;
- (3) MAI > 1.

Figure 19 exemplifies three zones with different mining activity (iron, base metals, industrial minerals, coal) and where sites from construction materials (both categories represented by their point coordinate and buffer) are also present. The catchments in the second and third MAI class correspond to those with overlaying CORINE mining-related polygons (mineral extraction sites, dumps, and industrial units), while most of the catchments containing only buffers of sites for construction material are classified in the first class of no hazard. There was a good global correspondence with the sites labeled as being most risky in the national mining monitoring system of Slovakia (Vrana *et al.*, 2005). Besides known sites, there are also catchments highlighted in the second and/or third MAI class, where no evidence of mining activity was available, so it might be worthy to investigate the cause of OH-FeOx anomalies.

The proposed classification scheme of catchments or other reference surfaces is to be considered in a first approach. The most critical factor in the MAI equation (1) is the great variation of the area of the reference surface. For a very small inter-basin with several highly anomalous pixels, a large value of normalized MAI could be obtained. The catchments in figure 19 are derived from a DEM of 250 m resolution, almost 10 times coarser than Landsat TM. However, their classification according to the proposed MAI is useful for differentiating the catchments with deposited mining materials with respect to the extent and types of occurring OH-FeOx anomalies. The catchments belonging to class 2 and 3 should be subsequently grouped according to size and/or other morphological criteria and a multiple-criteria decision could be then applied for further discrimination. Some of the decision rules could consist, for example, in: **1**) OH-FeOx anomalies as proportion of the area; **2**) proportion of highly anomalous pixels in total anomalous pixels etc. Some other criteria could be added later, such as the geology of the host rock, the mined commodity, the type of waste etc., for a better source characterization, needed for vulnerability studies and risk assessment.

## 5. CONCLUSIONS

The study showed that the method proposed for mapping mining wastes over large areas by a combination of PCs indicating zones enriched in iron oxides and hydroxyl-bearing minerals gave consistent results for all test sites. It is straightforward, semi-automated and can be run in an operational way on atmospherically and geometrically corrected Landsat TM (ETM) scenes.

The areas with iron oxides were mapped by a fourth and third order PCs. While Fe-PC4 highlighted the mining-related features showing raise in TM3 compared to TM1, Fe-PC3 also highlighted, due to its identical sign of eigenvector loadings in TM1 and TM3, the materials with flat spectral curves in the visible range, or even a decrease in TM3 compared to TM1. Having greater data variance than the fourth order component and high eigenvector loadings in TM3 and TM1, this PC3 also mapped the areas of iron staining highlighted by the former.

The combination of these two Fe PCs with OH-PC4 (pointing out areas with absorptions in TM7 against TM5) led to OH-FeOx anomaly images with 20 classes, which showed good correspondence with mining-related features according to the CORINE land cover database, national mining databases, paper maps and other ancillary available information.

Some filters based on reflectance values in atmospherically corrected bands to compensate for effects of turbid/eutrophic water, mixture soil - vegetation (in a particular phenological state) and bare soils were necessary to compensate for the coarse spectral resolution of TM/ETM and the presence of mixed pixels. Application of the method on regional scale therefore requires as imperiously necessary the use of atmospherically corrected images.

The suitability of the OH-FeOx anomalies for mapping mining wastes was proven through a statistical analysis. The maximum percentage of area covered by: **1**) all anomaly classes; **2**) the highly anomalous classes (i.e. 13 to 20 – Fig. 8); occur both in the case of mining-related features of CORINE land cover and national databases. Furthermore, the highly anomalous classes occur with the highest proportion (of total anomalies) in the mining-related features. On the contrary, the simple oxidation anomalies (classes 1 to 8 – Fig. 8) have a uniform distribution in all land cover classes, being by far prevalent in agricultural areas (bare soils).

The proposed Mining Anomaly Index, based on this observed differentiation of OH-FeOx anomalies, succeeded in a rough classification of first order catchments of Slovakia regarding the extent and broad type of deposited mining material, corresponding to the national mining monitoring system (Vrana *et al.*, 2005). This classification can be further developed using multiple criteria decision analysis, leading to a final risk-based inventory of mining and industrial associated contaminated sites.

In view of the present increased demand for metals and critical raw materials required by the technological developments of the 2020s, when European countries begin to reopen their mines, and the new modern techniques allow recovering of useful minerals from dumps and tailing ponds, the principles of the described methodology could be applied on atmospherically corrected images from the new satellite sensors, Landsat Operational Land Imager (OLI) and Sentinel 2 Multi-Spectral Instrument. (MSI). These satellite

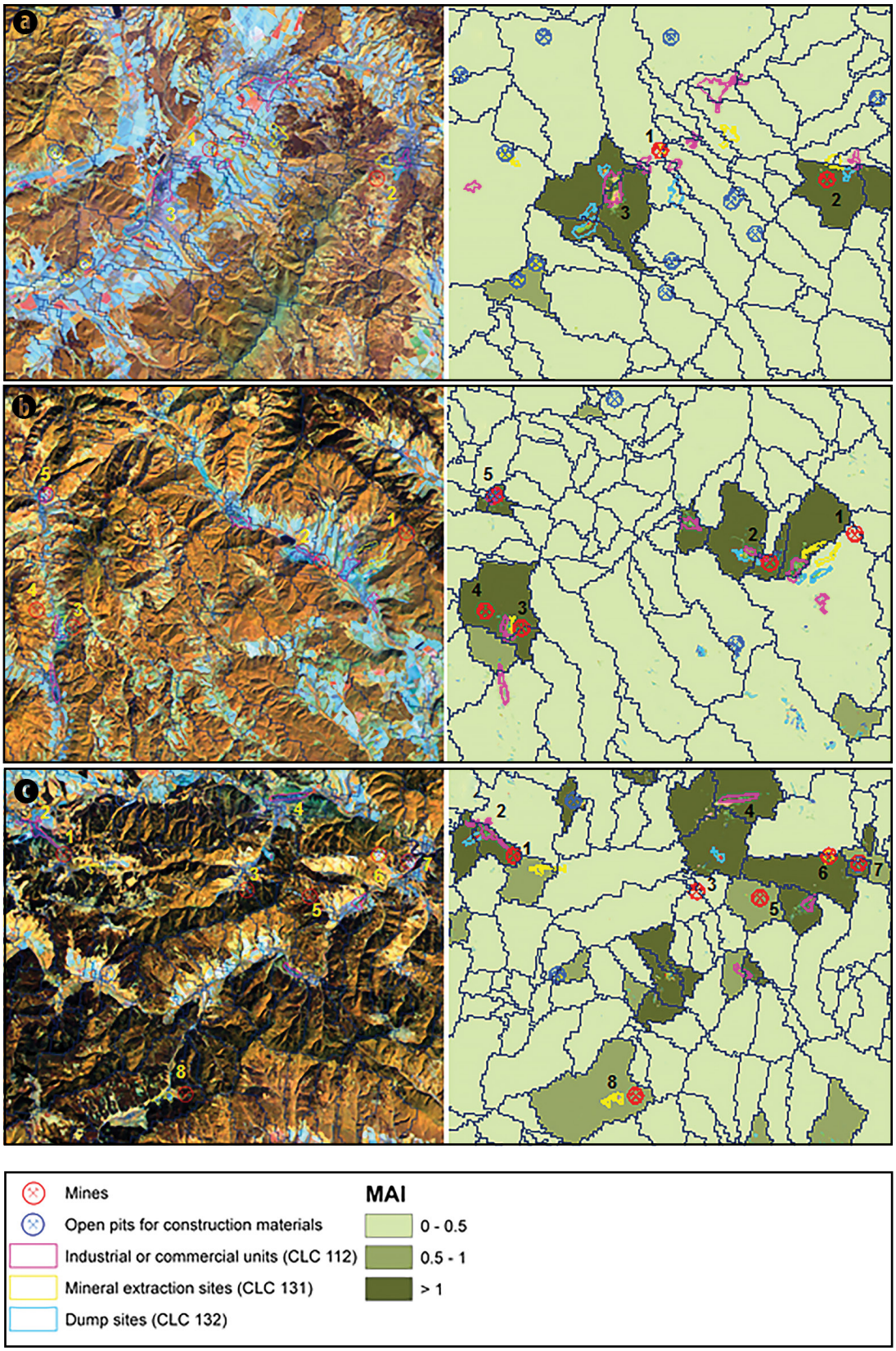


**Fig. 19.** Classification of first order catchments of Slovakia according to the Mining Anomaly Index. Exemplification for three selected areas, validated against national mining monitoring system (Vrana *et al.*, 2005). **a**) Nováky (brown coal mine and power plant); **b**) Jelšava, Lubeník (magnesite); Hnúšťa – Mútnik, Hačava (talc); Tisovec-Čremošné (limestone, dolomite); **c**) Rudňany – Poráč (baryte, iron and smelter); Smolník (iron, copper, antimony); Krompachy (smelter); Gelnica (iron, copper, mercury); Jaklovce (limestone, dolomite).

sensors have better ground and spectral resolution, and it is logical to expect that our method could be used in a more straightforward way, making use of the more dedicated spectral bands they possess.

## ACKNOWLEDGEMENTS

We are grateful to all our colleagues from the Joint Research Centre of the European Commission who contributed by making available pan-European data sets (IMAGE2000, CORINE Land Cover, CCM, etc.), our collaborators in Pecomines1 and 2 projects from the *Rural, Waters and Ecosystem Resources Unit* of the *Institute for Environment and Sustainability*, JRC, and our partners and members of the Steering Committees of the projects, who provided invaluable help by the offered information, suggestions and validation data.

## REFERENCES

Borcoș, M., Peltz, S., Stan, N., Marinescu, F., Săndulescu, M., Țicleanu, N., Bandrabur, T., Stanciu, C. (1980). Geological map 1:50.000, Seini (6d; L-34-11-D). Institute of Geology and Geophysics, Bucharest.

CEC Commission of the European Communities (1993). CORINE Land Cover - Guide Technique. Office for Official Publications of the European Communities, Luxembourg. EUR 12585, 144 p.

Constantinescu, E., Anastasiu, A., eds. (2017). Mineral Resources of Romania, Vol II. Metallic minerals and ores. Publishing House of the Romanian Academy, Bucharest, 2017, 631 p., ISBN 978-973-27-2810-9 (in Romanian).

Crosta, A.P., McMoore, J. (1989). Enhancement of Landsat Thematic Mapper Imagery for Residual Soil Mapping in SW Minais Gerais State, Brasil: A Prospective Case History in Green Stone Belt Terrain. *Proceedings of the 7th (ERIM) Thematic Conference – Remote Sensing for Exploration Geology*, Calgary, Oct. 2-6 1989: 1173-1187.

European Parliament and Council (2006). Directive 2006/21/EC of 15 March 2006 on the management of waste from extractive industries and amending Directive 2004/35/EC. *Official Journal of the European Union*, **L 102**: 15-33.

Hill, J. (1993). High Precision Land Cover Mapping and Inventory with Multi-Temporal Earth Observation Satellite Data. The Ardèche Experiment. EUR 15271 EN, Office for Official Publications of the European Communities, Luxembourg.

Hill, J., Mehl, W. (2003). Geo- und radiometrische Aufbereitung multi- und hyperspektraler Daten zur Erzeugung langjähriger kalibrierter Zeitreihen. *Photogrammetrie, Fernerkundung, Geoinformation* **1**/2003. S. 7-14, 3 Abb.: 7-14.

Hunt, G.R., Salisbury, J.W. (1970). Visible and near-infrared spectra of minerals and rocks: I silicate minerals. *Modern Geology*, **1**: 283-300.

Hunt, G.R., Salisbury J.W. (1971a). Visible and near-infrared spectra of minerals and rocks: II carbonates. *Modern Geology*, **2**: 23-30.

Hunt, G.R., Salisbury, J.W., Lenhoff, C.J. (1971b). Visible and near-infrared spectra of minerals and rocks: III oxides and hydroxides. *Modern Geology*, **2**: 195-205.

Hunt, G.R., Salisbury, J.W., Lenhoff, C.J. (1971a). Visible and near-infrared spectra of minerals and rocks: IV sulphides and sulphates. *Modern Geology*, **3**: 1-14.

Hunt, G.R., Salisbury, J.W., Lenhoff, C.J. (1972). Visible and near-infrared spectra of minerals and rocks: V halides, phosphates, arsenates, vanadates and borates. *Modern Geology*, **3**: 121-132.

Hunt, G.R., Salisbury, J.W., Lenhoff, C.J. (1973a). Visible and near-infrared spectra of minerals and rocks: VI aditional silicates. *Modern Geology*, **3**: 85-106.

Hunt, G.R., Salisbury, J.W., Lenhoff, C.J. (1973b). Visible and near-infrared spectra of minerals and rocks: VII acidic igneous rocks. *Modern Geology*, **4**: 217-224

Hunt, G.R., Salisbury, J.W., Lenhoff, C.J. (1974a). Visible and near-infrared spectra of minerals and rocks: VIII intermediate igneous rocks. *Modern Geology*, **4**: 237-244

Hunt, G.R., Salisbury, J.W., Lenhoff, C.J. (1974b). Visible and near-infrared spectra of minerals and rocks: IX basic and ultrabasic igneous rocks. *Modern Geology*, **5**: 15-22.

Hunt, G.R., Salisbury, J.W. (1976a). Visible and near-infrared spectra of minerals and rocks: XI sedimentary rocks. *Modern Geology*, **5**: 211-217.

Hunt, G.R., Salisbury, J.W. (1976b). Visible and near-infrared spectra of minerals and rocks: XII metamorphic rocks. *Modern Geology*, **5**: 219-228.

Hunt, G.R. (1980). Electromagnetic Radiation: The Communication Link in Remote Sensing. *In*: Siegal B.S., Gillespie A.R. (1980), Remote Sensing in Geology, John Wiley & Sons, Inc., New York, Singapore, Toronto.

Jánová, V., Vrana, K. (2004). Mining, Mining Waste and Related Environmental Issues in Slovakia. *In*: G. Jordan and M. D'Alessandro (eds.), Mining, Mining Waste and Related Environmental Issues: Problems and Solutions in Central and Eastern European Candidate Countries. *EUR Report 20661 EN*, Joint Research Centre of the European Commission, Ispra.

Kasinsky, J., Gientka, M. (2004). Mining, Mining Waste and Related Environmental Issues in Poland. *In*: G. Jordan and M. D'Alessandro (eds.), Mining, Mining Waste and Related Environmental Issues: Problems and Solutions in Central and Eastern European

Candidate Countries. *EUR Report 20661 EN*, Joint Research Centre of the European Commission, Ispra.

Kasinsky J., Gientka M., Korcz M., Krupanek J. (2007). Databases and maps of mining sites in Upper Silesia region. *In*: Pilot project "Regional Risk Assessment of Mining Sites and Contaminated Sites in the Upper Silesia Region". *Interim Report*, DG-JRC contract No. 381358-F1SC.

Lacaze, B., Caselles, V., Coll, C., Hill, J., Hoff, C., de Jong, S., Mehl, W., Negendank, J.F.W., Riezebos, H., Rubio, E., Sommer, S., Teixeira Filho, J., Valor, E. (1996). Integrated Approaches to Desertification Mapping and Monitoring in the Mediterranean Basin. *Final Report of the DEMON-1 Project. EUR 16448 EN*, Office for Official Publications of the European Communities, Brussels, Luxembourg, 1993.

Loughlin, W.P. (1990). Geological Exploration in the Western United States by Use of Airborne Scanner Imagery. *IMN Conference "Remote Sensing – An Operational Technology for Mining and Petroleum"*, London, Oct. 29-31, 1990: 223-241.

Loughlin, W.P. (1991). Principal Component Analysis for Alteration Mapping. *Photogramm. Eng. Rem. Sens.*, **57**(*9*): 1163-1169.

Mustard, J. F., Sunshine, J.M. (1999). Spectral Analysis for Earth Science: Investigations Using Remote Sensing Data. *In*: Rencz, A. N. (ed) (1999). Remote Sensing for the Earth Sciences: Manual of Remote Sensing, third edition, vol. 3, John Wiley &Sons, Inc.

Sommer, S., ed. (2004). Options for Compiling an Inventory of Mining Waste Sites throughout Europe. Based on the conclusions from the JRC Enlargement Project PECOMINES - Inventory, Regulations and Environmental Impact of Toxic Mining Wastes in Pre-Accession Countries. EUR 21186 EN, Joint Research Centre of the European Commission, Ispra.

Swayze, G.A., Clark, R.N., Pearson, R.M., Livo, K.E. (1996). Mapping Acid-Generating Minerals at the California Gulch Superfund Site in Leadville, Colorado using Image Spectroscopy. *Summaries of the 6th Annual JPL Airborne Earth Science Workshop*, March 4-8, 1996

Tanré, D., Deroo, C., Duhaut, P., Herman, M., Morcrette, J.J., Perbos, J., Deschamps, P.Y. (1990). Description of a computer code to simulate the signal in the solar spectrum: the 5S code. *Int. J. Remote Sensing*, **11**(*4*): 659-668.

Veliciu, S., Stratulat, P. (2004). Mining, Mining Waste and Related Environmental Issues in Romania. *In*: G. Jordan and M. D'Alessandro (eds.), Mining, Mining Waste and Related Environmental Issues: Problems and Solutions in Central and Eastern European Candidate Countries. *EUR Report 20661 EN*, Joint Research Centre of the European Commission, Ispra.

Vijdea, A.-M., Sommer, S., Mehl, W. (2004). Use of Remote Sensing for Mapping and Evaluation of Mining Waste Anomalies at National to Multi-Country Scale in Pre-Accession Countries. *EUR 21185 EN*, Joint Research Centre of the European Commission, Ispra, ISBN 92-894-7792-X.

Vrana, K., Vojtaško, I., Žák, D., Piovarči, M., Puchnerová, M., Lanc, J. (2005). Systém zisťovania a monitorovania škôd na životnom prostredí vznikajúcich banskou činnosťou (System of detection and monitoring of environmental impacts caused by mining activities). Final Report – Manuscript, Ministry of Environment of the Slovak Republic – Geocomplex Inc. Bratislava (in Slovak).